MULTILAYER ROADWAY CONDITION EVALUATION USING NDT AND DEEP LEARNING IMPLEMENTATION

By

AHMAD MAHDI ABDELMAWLA

(Under the Direction of SUNG-HEE 'SONNY' KIM)

ABSTRACT

This research represents a comprehensive exploration of the utilization of Ground Penetrating Radar (GPR) technology and advanced deep learning models in the assessment of civil engineering infrastructure, with a particular focus on road construction and pavement maintenance. The research comprises two distinct yet interrelated components: the development of the GPR-Density model for subgrade layer evaluation and the introduction of the GPR-YOLOR model for subsurface distress detection. Together, these components provide novel and practical solutions to long-standing challenges in infrastructure assessment.

The GPR-Density model offers a non-invasive means to assess subgrade layer physical parameters, notably dry density, contributing to more accurate and efficient construction quality control. The model derives from a robust mathematical framework, involving the relationship

between the dielectric constant of soil and its density, among other properties. Calibration in laboratory settings, combined with field test validation, demonstrates the model's potential for accurately estimating soil properties, particularly for fine-grained soil types. The research highlights the feasibility of using GPR to predict subgrade dry density and paves the way for future investigations into network-level road assessment.

In parallel, the GPR-YOLOR model, integrated with various image enhancement techniques, revolutionizes pavement assessment by enhancing the reliability and speed of subsurface distress detection. This deep learning framework, known for its speed and accuracy, utilizes high-resolution GPR images to detect and classify pavement cracks and abnormalities. The model's real-world implementation is underscored by extensive field tests and validation, ensuring its applicability and effectiveness in practical scenarios. Furthermore, the study explores the potential integration of GPR data with other non-destructive testing technologies, offering a more comprehensive assessment of infrastructure health.

While this research marks significant advancements in GPR-based infrastructure assessment, it acknowledges limitations, including the need for expanded datasets, refined image enhancement techniques, and a focus on the mechanical properties of pavement layers. These challenges provide fertile ground for future research, ensuring the continuous evolution of non-destructive testing methodologies in civil engineering. Integrating remote sensing and satellite imagery analysis techniques with GPR reflection calculations is also proposed as an innovative avenue for large-scale infrastructure monitoring and management.

In summary, this research not only contributes to the field of civil engineering and pavement infrastructure assessment but also serves as a testament to the potential of emerging

technologies and methodologies in addressing critical challenges in maintaining and managing vital infrastructure assets.

INDEX WORDS: Ground penetrating radar (GPR), non-destructive testing (NDT), pavements, dielectric constant, Machine Learning, Artificial Intelligence

MULTILAYER ROADWAY CONDITION EVALUATION USING NDT AND DEEP LEARNING IMPLEMENTATION

By

Ahmad Mahdi Abdelmawla

B.S., Cairo University, Egypt, 2011

M.S., Cairo University, Egypt, 2017

A Dissertation Submitted to the Graduate Faculty of The University of Georgia in Partial Fulfillment of the Requirements for the Degree

DOCTOR OF PHILOSOPHY

ATHENS, GEORGIA

MULTILAYER ROADWAY CONDITION EVALUATION USING NDT AND DEEP LEARNING IMPLEMENTATION

by

Ahmad Mahdi Abdelmawla

Major Professor: S. Sonny Kim

Committee: Stephan A. Durham

James J. Yang

Ben Davis

Bjorn Birgisson

Electronic Version Approved:

Ron Walcott

Dean of the Graduate School

The University of Georgia

December 2023

DEDICATION

This dissertation is dedicated to

First and foremost, to Allah (God), who said in His holy book:

17:85 And they ask you (O Muhammad SAW) concerning the Ruh (the Spirit); Say: "The Ruh (the Spirit): it is one of the things, the knowledge of which is only with my Lord. And of knowledge, you (mankind) have been given only a little."

In His infinite wisdom, Allah reminds us that knowledge is boundless, urging us to seek it tirelessly. It is through His divine guidance that I have been able to demonstrate my capabilities and find success in this academic endeavor.

To my beloved wife, whose unwavering love and steadfast support have been a constant source of motivation throughout this challenging journey. Her presence and encouragement have been my pillars of strength.

Additionally, I extend this dedication to my parents, whose unwavering belief in my abilities, as well as their boundless love and dedication, have shaped me into the person I am today. Their commitment to instilling life ethics and values in me has been an invaluable gift.

I am truly blessed to have such a support system, and this dissertation stands as a tribute to their steadfast faith in me.

ACKNOWLEDGEMENTS

I would like to express my heartfelt gratitude to Professor Dr. S. Sonny Kim for his unwavering support, invaluable guidance, and the trust he placed in me throughout the entire research process. Dr. Kim's mentorship has been pivotal in shaping this research, and I am deeply appreciative of his dedication to my academic growth.

I also extend my sincere thanks to the members of my committee for their understanding and guidance, which have been essential in refining this research to its current format and value. Your expertise and insights have played a crucial role in shaping this work.

I am indebted to the University of Georgia for its unwavering support and for providing the necessary facilities and sponsorship that enabled the development of innovative research ideas. The university's commitment to fostering research excellence has been a cornerstone of this project's success.

I would like to acknowledge the Georgia Department of Transportation for its visionary leadership and cooperation with the University of Georgia. Their partnership has allowed us to conduct research that not only benefits the community but also leads the industry towards enhanced performance and innovation.

Additionally, I extend my appreciation to my lab colleagues for their invaluable assistance during both laboratory and field work. Your collaboration and support have been crucial in achieving the objectives of this research.

TABLE OF CONTENTS

LIST OF TABLES

LIST OF FIGURES

CHAPTER 1

INTRODUCTION

1.1. OVERVIEW

Over the past decades, humanity has witnessed remarkable technological advancements that have revolutionized various fields. However, when it comes to the investigation and assessment of pavement stability, progress has been notably slow. Despite the wealth of technological knowledge accumulated, pavement investigation methods continue to lag behind. From this perspective, this research represents a groundbreaking contribution to the field of pavement infrastructure testing. It achieves this by delicately merging the capabilities of Non-Destructive Testing (NDT) techniques with the transformative power of Artificial Intelligence (AI). In doing so, it endeavors to usher in a new era of innovative and accelerated pavement assessment methodologies.

1.2. BACKGROUND

1.2.1. Transportation infrastructures

Transportation infrastructures play a crucial role in facilitating the movement of people and goods, supporting economic development, and connecting communities. Among the essential components of transportation networks, pavement structures form the backbone of road systems. Pavements, engineered structures designed to bear vehicle loads, are fundamental in ensuring safe

and efficient travel for both passenger and freight traffic. The importance of well-built and properly maintained pavements has been recognized for centuries.

Throughout history, civilizations have recognized the significance of purpose-built pavement structures. Examples can be traced back to ancient times, such as stone-paved streets in the Middle East and wooden log surfaced roads in England dating back to 4000 B.C. Additionally, brick paving in India around 3000 B.C. showcases early engineering achievements (Lay, 1992). The Roman Empire is renowned for its extensive network of approximately 78,000 kilometers of paved roads, showcasing the value placed on sound pavement engineering. In fact, the Roman practice of constructing roads on raised embankments gave rise to the term "highway." These historical examples highlight the enduring importance of well-constructed pavements (O'Flaherty, 2002).

Maintaining resilient pavement structures is of utmost importance to ensure their long-term functionality and minimize disruptions. Continuous testing and maintenance operations play a critical role in achieving this goal. Non-destructive testing methods, such as ground penetrating radar (GPR), have emerged as valuable tools for assessing pavement conditions without causing significant disruptions to traffic flow. By identifying potential issues and conducting timely repairs or rehabilitation, transportation authorities can ensure the resilience and durability of pavement structures.

In this dissertation, the research delves into the significance of transportation infrastructures, with a specific focus on pavement structures. By exploring non-destructive testing techniques, particularly GPR, the aim is to enhance pavement investigation capabilities and improve the understanding of pavement conditions. Through this research, main goal is to contribute to the development of more efficient and cost-effective methodologies for evaluating and maintaining

resilient pavement structures, ultimately benefiting transportation networks and supporting sustainable economic growth.

1.2.2. Non-destructive testing

Non-destructive testing (NDT) has become essential for assessing the structural integrity and quality of pavements in modern road infrastructures. By utilizing NDT methods, pavement inspections can be conducted thoroughly without causing damage or disrupting traffic. NDT plays a crucial role in detecting defects, assessing material strength, verifying dimensions, and ensuring compliance with quality standards, all of which contribute to the maintenance of safe and durable road surfaces (Plati et al. 2020).

Traditionally, assessing pavement conditions involved invasive and time-consuming procedures that had limitations in terms of cost, accuracy, and real-time information capture. To address these limitations, there has been a shift towards non-destructive testing methods in pavement inspections. NDT systems offer non-invasive approaches to assess pavements, providing valuable data on geometric measurements, cracking detection, thickness estimation, roughness evaluation, and mechanical property assessment. These methods minimize disruptions, reduce maintenance costs, and offer more reliable and timely information for informed decision-making.

By integrating NDT into routine pavement analysis, transportation authorities and engineers can detect defects early, evaluate material strength, and optimize maintenance schedules. This proactive approach to pavement inspections leads to safer roadways, cost savings, and improved infrastructure durability, benefiting road users and supporting economic growth.

1.3. PROBLEM STATEMENT

With the rapid growth of urban areas and increasing population in the past two decades, there is an urgent need to establish and maintain robust and sustainable road infrastructure. However, the conventional process of conducting road scans for maintenance purposes and evaluating the condition of multiple layers proves to be a costly, resource-intensive, time-consuming, and potentially hazardous endeavor, particularly on highly trafficked roads. This raises a critical inquiry: Is there a methodology available that offers a swifter, more dependable, and cost-effective approach to assessing the condition of road structures, encompassing both surface and subgrade layers?

The primary objective of this research is to address this fundamental question by harnessing the capabilities of ground-penetrating radar (GPR) technology, in conjunction with advanced deep learning algorithms. By integrating GPR and deep learning techniques, there exists a promising opportunity to provide a prompt and reliable solution to the challenges associated with evaluating road structure conditions. Through the utilization of non-destructive testing (NDT) methods and the application of deep learning models, it becomes feasible to undertake efficient and cost-effective assessments of multilayer roadways.

This research aims to explore and develop a comprehensive methodology utilizing GPR technology and advanced deep learning algorithms for evaluating the condition of road structures, encompassing both surface and subsurface layers. The ultimate goal is to offer road authorities, traffic engineers, and infrastructure managers an innovative approach that significantly enhances the speed, accuracy, and affordability of road condition assessments. Consequently, the outcome of this research will contribute to the advancement of sustainable road infrastructure by enabling timely and well-informed decision-making in maintenance and rehabilitation endeavors.

1.4. RESEARCH OBJECTIVES

The primary aim of this research is to enhance pavement investigation capabilities by improving the methodologies and procedures used to analyze information obtained from ground-penetrating radar (GPR) scans. In order to achieve this aim, the following research objectives have been identified:

1. To enhance the analysis and interpretation of GPR scan data for pavement evaluation: This objective involves developing advanced algorithms and techniques to extract relevant information from GPR scans and accurately assess the condition of road structures, including surface and subsurface layers. The focus will be on refining existing methodologies and exploring novel approaches to improve the accuracy and reliability of GPR data analysis.
2. To characterize subgrade soil physical properties using GPR road scan results: This objective aims to investigate the potential of GPR technology in assessing subgrade soil properties. It involves developing methods to analyze GPR data specifically related to subgrade soil characteristics, such as soil moisture content, density, and layer thickness. The goal is to establish a correlation between GPR measurements and subgrade properties for more comprehensive road condition assessments.
3. To develop machine learning models for connecting surface images with GPR subgrade soil scanning analysis: This objective focuses on leveraging machine learning techniques to establish a relationship between surface images and GPR data related to subgrade soil conditions. By training deep learning models on a large dataset comprising surface images and corresponding GPR scans, the objective is to create a predictive model that can accurately classify road stress types, distinguishing between surface cracks and structural cracks.

1.5. RESEARCH SIGNIFICANCE AND SCOPE

The research conducted in this Ph.D. dissertation holds significant academic and practical significance in the field of pavement evaluation and road infrastructure management. The following points outline the research significance and scope:

- Advancement of GPR technology in pavement evaluation.
- Improved efficiency, accuracy, and affordability of road condition assessments.
- Support for sustainable road infrastructure development.
- Reduction in decision-making time for road rehabilitation.
- Application of remote sensing and machine learning in soil attribute modeling.

Overall, this dissertation significantly contributes to the academic understanding and practical implementation of GPR technology in pavement evaluation. It aims to improve the efficiency, accuracy, and affordability of road condition assessments, supporting sustainable road infrastructure development and reducing decision-making time for road rehabilitation projects. Additionally, the research explores the application of remote sensing and machine learning in soil attribute modeling, expanding the knowledge base in this area.

1.6. ORGANIZATION OF THE DISSERTATION

This dissertation is divided into seven chapters that describe soil properties importance in saltmarsh health and productivity, which include:

Chapter 1: Introduction

- Provides an overview of the research topic and background information.

- Discusses transportation infrastructures, non-destructive testing, and ground-penetrating radar.
- States the problem statement, research objectives, significance, and scope of the study.

Chapter 2: Literature Review

- Provides an overview of pavement structures and condition assessment methods.
- Reviews non-destructive testing applications and electromagnetic testing technology.
- Explores the theory and applications of ground-penetrating radar (GPR).
- Discusses the use of artificial intelligence and deep learning in pavement engineering.
- Highlights advancements in pavement distress prediction.

Chapter 3: Density Prediction Model

- Presents the theories and derivation of the GPR-density model.
- Describes the implementation of the model.
- Provides laboratory and field test results.
- Discusses the application and conclusion of the model.

Chapter 4: Subsurface Anomaly Detection

- Outlines the methodology for subsurface anomaly detection.
- Describes the deep learning model and data acquisition techniques.
- Presents the experiment results and conclusions.

Chapter 5: Subsurface Distress Prediction Field Validation

- Focuses on deep learning subsurface distress prediction.
- Describes image enhancement techniques for GPR and surface images.

- Introduces the GPR-YOLOR model and its implementation.
- Evaluates the model's performance.

Chapter 6: Conclusions and Recommendations

- Summarizes the findings of the research.
- Highlights the contributions to the field.
- Discusses the limitations of the study and provides recommendations for future research.

CHAPTER 2

LITERATURE REVIEW

2.1. OVERVIEW

Over the past few decades, road engineering activities have increasingly focused on the effective and efficient management of infrastructure assets through proper maintenance actions, while the demand for new constructions has shown a gradual decline. However, in developing countries, the demand for new infrastructure remains higher, as it is essential to establish basic connections to facilitate services like education, primary healthcare, water supply, local markets, and economic opportunities. This emphasis on economic development aims to bridge the gap between remote areas and urban centers, promoting overall progress.

In recent times, there has been a concerning trend of deteriorating sustainable operations and maintenance practices for these newly constructed infrastructures. Despite the availability of funding, there seems to be a lack of emphasis on maintenance, leading to a growing issue. Interestingly, maintenance practices are more widespread and prioritized. The disparity in maintenance approaches cannot be solely attributed to a lack of funding; rather, it highlights the existence of technical challenges, such as inadequate planning and insufficient information regarding the overall condition of the road network.

Addressing these issues is crucial to ensure the longevity and sustainability of road infrastructure. Proper maintenance is vital to optimize the lifespan of existing infrastructure and to avoid costly

and extensive rehabilitation or reconstruction projects. Implementing effective maintenance strategies requires reliable data and information on the condition of the road network, enabling informed decision-making and resource allocation. By bridging the gap between planning and information, countries can better address their infrastructure maintenance needs and promote the development of a well-maintained and sustainable road network.

Modern pavement structures consist of multiple layers arranged systematically to achieve specific objectives. Watson (1994) defines the primary functions of a pavement as providing a safe, stable, and durable structure capable of withstanding the effects of weather and vehicular loading over an extended period. To fulfill these functions, pavements are constructed with a combination of layers, each serving a distinct purpose, as illustrated in Figure 1.

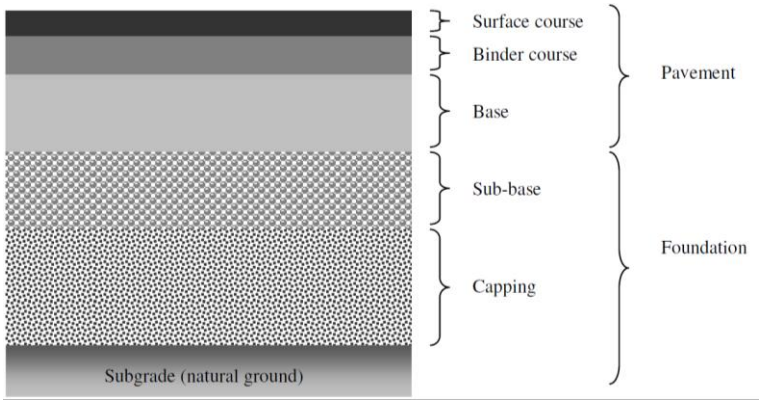

Figure 1 Pavement Structure layers layout (Evans, 2010)

Understanding the different types and components of pavement structures is critical for efficient and effective pavement design, construction, and maintenance. By considering the specific requirements of each application and selecting appropriate materials and layer configurations, engineers can develop pavements that meet the desired performance criteria and ensure the long-term sustainability of the infrastructure.

2.2. PAVEMENT CONDITION ASSESSMENT METHODS

Ensuring driving safety is a paramount concern within the field of pavement engineering, where the condition of pavement surfaces holds significant implications (Tighe et al., 2000). Cracks, potholes, and surface deformations on road pavements can induce sudden vertical accelerations experienced by vehicle tires, leading to a decrease in the effective friction between the tires and the pavement surface. Consequently, these road damages jeopardize driving safety by compromising vehicle stability and overall performance on the road (Tighe et al., 2000).

The occurrence of cracks, potholes, and surface deformations serves as indicators of pavement deterioration, often associated with a decrease in the bearing ratio of the load-bearing layers and subgrade soils (Diefenderfer et al., 2005). Several factors contribute to this reduction in bearing ratio, including inadequate design, poor construction practices, and the presence of excessive moisture in the sub-asphalt courses.

In response to these challenges, it is imperative to adopt effective measures for early detection and prevention of pavement distress through regular inspection and maintenance operations. Pavement condition assessment assumes paramount importance in the effective management of road infrastructure. Traditional assessment methods, such as visual inspection and asphalt coring, have been conventionally employed. However, nondestructive testing (NDT) techniques, such as the Falling Weight Deflectometer (FWD) and Ground Penetrating Radar (GPR), have emerged as favorable alternatives due to their inherent advantages in terms of efficiency and accuracy (TRL Report LR 833, Kennedy and Lister, 1978).

Visual inspection and coring methods involve manual field testing, which can be labor-intensive and time-consuming. In contrast, nondestructive testing methods offer the advantage of acquiring

valuable data without causing damage to the pavement itself. This nonintrusive nature of NDT minimizes disruptions to the pavement surface while providing valuable insights into its structural integrity and performance.

Among the various nondestructive testing techniques, FWD is widely utilized in assessing the deflection response of road pavements under load. Measured deflections obtained through FWD serve as primary criteria for evaluating the long-term performance of pavements (TRL Report LR 833, Kennedy and Lister, 1978). By establishing correlations between measured deflections and known traffic loading, it becomes possible to predict the future performance of pavements and estimate their residual life before necessitating interventions to prolong their useful lifespan.

In addition to FWD, GPR has emerged as a valuable nondestructive testing technique for pavement condition assessment. GPR employs electromagnetic waves to penetrate the pavement layers, providing detailed subsurface information regarding the pavement structure, including layer thickness, void presence, and moisture content. The utilization of GPR offers the advantage of assessing multiple pavement layers without the need for coring or excavation, thereby serving as a valuable tool for pavement maintenance engineers (TRL Report LR 833, Kennedy and Lister, 1978).

2.3. NON-DESTRUCTIVE TESTING APPLICATIONS

Non-destructive testing or evaluation (NDT/NDE) methods aim to detect and classify defects and damages in various materials without causing any destruction (Maierhofer, 2010). While quantifying the magnitude of these defects may not always be possible, NDT methods focus on determining the position and dimensions of heterogeneities when changes in physical properties occur within a homogeneous domain.

In recent years, non-destructive testing techniques have gained significant attention in the field of repair and maintenance across various applications. Concrete testing has been a common area of focus, with studies exploring techniques for assessing concrete quality and detecting internal defects (Beutel et al., 2008; Dérobert et al., 2008; Dérobert and Berenger, 2010). NDT methods have also been employed in the inspection and preservation of ancient buildings, addressing concerns related to structural integrity and historical conservation (Ranalli et al., 2004; Solla et al., 2011). Additionally, NDT techniques have been utilized for land use purposes, such as identifying underground structures and assessing soil conditions (Fenning and McCannt, 1995; Minet et al., 2011). Modern infrastructure safety, including the characterization of stone masonries and inspection of bridge decks, has also benefited from non-destructive testing approaches (Binda et al., 1998, 2005; Diamanti and Redman, 2012; Helmerich et al., 2012; Benedetto et al., 2012b; Hugenschmidt and Mastrangelo, 2006; Saarenketo and Soderqvist, 1994).

It is important to note that the application of NDTs can vary depending on the condition and age of the structure, as well as the specific stage of its life. Consequently, NDTs enable partial monitoring of the evolution of damage in a structure, providing valuable insights into its overall health and performance.

While conventional destructive methods are still utilized for calibration purposes in NDT measurements, technological advancements and research progress are gradually reducing the reliance on core sampling techniques (Maierhofer et al., 2010). This signifies a positive trend toward the development of non-destructive testing approaches that minimize damage to the inspected materials and improve the overall efficiency and accuracy of structural assessments.

Overall, non-destructive testing methods play a significant role in detecting and characterizing defects and damages in various materials. Their broad application across different fields and

structures highlights the potential for these techniques to enhance the understanding, preservation, and maintenance of diverse structures, contributing to the overall sustainability and safety of built environments. NDT encompasses various methodologies employed in the evaluation of pavements.

Ultrasonic methods, including Pulse Velocity Sonic Pavement Analyzer (PSPA) and Digital Sonic Pavement Analyzer (DSPA), are utilized to assess Hot Mix Asphalt (HMA) and unbound materials such as aggregate base and embankment soils. By utilizing ultrasonic waves, these methods analyze material properties considering factors such as moisture content and density.

Geo-Gauge, is a steady-state vibratory method, enables the determination of elastic modulus values for HMA and unbound materials. Its results are correlated with resilient modulus values obtained through laboratory testing or regression equations provided by programs like the Federal Highway Administration's Long-Term Pavement Performance (FHWA-LTPP). Moisture content and density significantly influence the Geo-Gauge measurements, contributing valuable insights into material stiffness.

The Falling Weight Deflectometer (FWD) applies dynamic loads to simulate heavy wheel loads on pavements. Measuring the deflection response of the pavement surface, the FWD facilitates the assessment of pavement stiffness, which is critical for evaluating structural integrity and load-carrying capacity.

For situations requiring portability and rapid measurements, the Light Weight Deflectometer (LWD) serves as a practical alternative to the FWD. This device allows for prompt deflection measurements, making it particularly suitable for field applications.

The Dynamic Cone Penetrometer (DCP) estimates the strength and modulus of unbound materials by conducting cone penetration tests. It quantifies the blows necessary to penetrate the material to a specific depth, establishing correlations with parameters derived from the Standard Penetration Test (SPT). While the DCP offers simplicity, mobility, and cost-effectiveness, it is relatively slower and physically demanding compared to other methods.

Ground Penetrating Radar (GPR) employs radio waves to measure pavement layer thicknesses and properties. This non-destructive technique penetrates the pavement structure, generating echoes at boundaries between different materials. GPR offers rapid data collection at speeds up to 40 miles per hour, providing valuable insights into pavement quality. Interpretation of GPR data necessitates skilled operators and specialized software, which generate visual representations of the pavement system.

Electric current and electronic methods employ technologies like electrical sensing fields and radio waves to assess the quality of HMA pavement, base, and embankment materials. The Electrical Density Gauge measures density of unbound layers by inserting 6-inch darts into the soil within a defined area, particularly applicable to aggregate base layers and embankments. The Pavement Quality Indicator (PQI) rapidly measures pavement density variations using a constant voltage, radio frequency, electrical impedance approach. By detecting changes in the dielectric constant through an electrical sensing field, the PQI provides insights into density variations. The PaveTracker, an electric current-based method, swiftly measures the uniformity of HMA mixtures, facilitating the timely detection of segregation, lower density levels along longitudinal joints, or other non-uniformity issues during construction.

Moreover, electromagnetic testing technology – like GPR – offers notable advantages over other methods. It enables non-contact and non-destructive assessment of pavements, eliminating the

need for physical contact with the surface and minimizing potential damage. Electromagnetic testing also provides rapid data acquisition, allowing for efficient evaluation of large pavement areas along with subsequent subsurface layers. Additionally, electromagnetic methods offer the ability to measure properties such as moisture content and layer thicknesses, expanding the scope of information obtained during the evaluation process. These advantages contribute to the growing popularity and effectiveness of electromagnetic testing technology in the field of pavement assessment.

2.4. ELECTROMAGNETIC TESTING TECHNOLOGY

Electromagnetic (EM) techniques in pavement assessment rely on the analysis of electromagnetic wave propagation velocity within materials. This analysis is based on the transmission and reflection of short electromagnetic impulses emitted and detected by antenna systems. The propagation velocity of EM waves is governed by the dielectric permittivity of the material, with moisture content playing a significant role in influencing its value. Additionally, the conductivity and dielectric losses of the material impact the attenuation of electromagnetic wave energy.

EM waves are composed of alternating electrical and magnetic fields that originate from oscillating electrical charges. The behavior of radar signals as they pass through materials adheres to the fundamental principles governing EM wave propagation. The EM spectrum encompasses various wave types characterized by their frequency, measured in cycles per second (Hz). The frequency, together with the velocity of wave propagation in a material, determines its wavelength. The EM spectrum ranges from gamma waves with high frequencies and short wavelengths of approximately 0.01 nm (0.01×10^{-9} m) to radio waves with low frequencies and long wavelengths in the order of 1.0 km. While radar is initially associated with radio frequency waves, modern

Ground Penetrating Radar (GPR) systems operate at the lower end of the microwave frequency range, typically featuring wavelengths on the scale of a few centimeters.

Dielectric substances are characterized by their limited electrical conductivity but the ability to support electric fields. The response of a material to an EM wave is influenced by its dielectric properties, which include electrical permittivity (ε), magnetic permeability (μ), and electrical conductivity (σ).

By exploiting the interaction between EM waves and dielectric properties, EM techniques enable non-contact and non-destructive assessment of pavement layers. The ability to analyze the propagation velocity and attenuation of EM waves provides valuable insights into the material composition, moisture content, and structural integrity of pavements. This information aids in the effective management and maintenance of road infrastructure, contributing to enhanced safety and durability.

2.5. GROUND PENETRATING RADAR

The application of Ground Penetrating Radar (GPR) in pavement investigations has experienced significant development since the early 1980s, establishing itself as a widely recognized technique in many countries. The initial use of GPR in traffic infrastructure surveys dates to the 1970s when the U.S. Federal Highway Administration (FHWA) employed it for testing in tunnel applications. Subsequently, in 1985, the FHWA pioneered the development of the first vehicle mounted GPR system specifically designed for highway applications. GPR has proven effective in various pavement investigation tasks, providing essential information for pavement assessment. Its key advantages include its nondestructive nature, cost-effectiveness compared to traditional methods, high-speed and continuous data acquisition capabilities, and reliability. When compared to other

geophysical technologies such as seismic, transient electromagnetic, electrical, and magnetic approaches, GPR stands out for its ability to deliver accurate and high-resolution data. However, it should be noted that GPR performance may be limited in the presence of high-conductivity materials such as clay or salt-contaminated soils, as well as in heterogeneous conditions that give rise to complex electromagnetic-scattering phenomena.

GPR finds wide-ranging applications in the field of civil engineering for inspection, monitoring, and design purposes. Its main uses include utility and buried object detection, surveying road pavements, bridge decks, and tunnels, as well as measuring moisture content in natural soils and artificial materials. In pavement investigations, GPR has been successfully applied to determine pavement layer thickness and identify subsurface defects. Standard GPR systems typically operate using impulse frequencies, where a single electromagnetic wave at a selected frequency is utilized.

The theoretical foundations of GPR are rooted in electromagnetic (EM) theory, which has a history spanning over two centuries and is extensively covered in various texts. To work quantitatively with GPR, it is necessary to understand the fundamental principles of EM wave propagation, as depicted in Figure 2. Although all GPR systems operate based on these principles, different types of GPR systems exploit various aspects of EM wave propagation and employ distinct hardware and data processing procedures.

The main components of an impulse GPR system, as illustrated in Figure 2, include an antenna unit with a transmitter and receiver, a control unit, a data console or display, and a power unit. Impulse GPR systems function by transmitting a brief burst or "pulse" of EM energy from a transmitter and capturing the reflections of the pulse as it encounters features or layers within the pavement using a receiver.

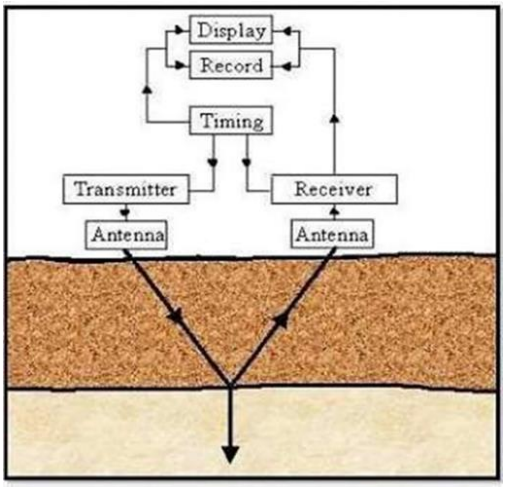

Figure 2 GPR theoretical application

GPR serves as a valuable tool in pavement investigations, offering nondestructive data collection, cost-effectiveness, and reliable results. Its wide range of applications and its ability to provide accurate and high-resolution information make it an indispensable technology in pavement assessment and management.

2.5.1. Electromagnetic Theory for GPR

Maxwell's equations form the cornerstone of electromagnetic (EM) theory as they mathematically describe the behavior of EM fields. These equations provide a comprehensive framework for understanding how electric and magnetic fields interact and propagate. Constitutive relationships, on the other hand, establish the connection between EM fields and material properties. These relationships allow us to quantify the response of materials to EM fields, such as their electrical conductivity, dielectric permittivity, and magnetic permeability. By combining Maxwell's equations with constitutive relationships, a quantitative understanding of the signals obtained can be developed in Ground Penetrating Radar (GPR) applications. This integration of theory and material properties forms the basis for interpreting GPR data and extracting valuable information about subsurface structures and properties.

Mathematically, EM fields and their relationships are described by equations 1, 2, and 3:

$$\bar{\nabla}.\bar{E} = -\frac{\partial \bar{B}}{\partial t} \quad (2\text{-}1)$$

$$\bar{\nabla}.\bar{D} = q \quad (2\text{-}2)$$

$$\bar{\nabla}.\bar{B} = 0 \quad (2\text{-}3)$$

Where,

$\bar{E}$: electric field strength vector (V/m), $\bar{J}$: electric current density vector (A/m^2),

q : electric charge density (C/m^3), $\bar{D}$: electric displacement vector (C/m^2),

$\bar{B}$: magnetic flux density vector (T), $\bar{H}$: magnetic field intensity (A/m),

t : time (s).

Equation (2-1) relates the divergence of the electric field ($\bar{E}$) to the negative time derivative of the magnetic field ($\bar{B}$). It represents the relationship between electric and magnetic fields and their variation over time. Equation (2-2) expresses the divergence of the electric displacement field ($\bar{D}$) in terms of the electric charge density (q). It relates the presence of electric charges to the distribution of electric fields. Equation (2-3) states that the divergence of the magnetic field ($\bar{B}$) is zero, indicating that magnetic field lines are closed loops and do not have sources or sinks.

These equations form the foundation for understanding the behavior of electromagnetic fields and their interactions with charges and currents in each space. By solving these equations in specific contexts, such as in the presence of different materials, one can obtain valuable insights into the properties and behavior of EM fields.

2.5.2. GPR Constitutive Relationship

Constitutive relationships are vital for characterizing material responses to EM fields, particularly in GPR applications. Equations (2-4), (2-5), and (2-6) provide a macroscopic description of how

electrons, atoms, and molecules within a material react to an EM field. Understanding these relationships is essential for GPR scan analysis and interpreting electromagnetic wave fields.

$$\bar{J} = \tilde{\sigma}\bar{E} \tag{2-4}$$

$$\bar{D} = \tilde{\varepsilon}\bar{E} \tag{2-5}$$

$$\bar{B} = \tilde{\mu}\bar{H} \tag{2-6}$$

Where,

$\tilde{\sigma}$: electrical conductivity that characterizes free charge movement (creating electric current) when an electric field is present.

$\tilde{\varepsilon}$: dielectric permittivity that characterizes displacement of charge constrained in a material structure to the presence of an electric field.

$\tilde{\mu}$: magnetic permeability, which describes how intrinsic atomic and molecular magnetic moments respond to a magnetic field.

These constitutive relationships provide insights into material behavior and their interaction with EM fields. Equation 4 relates electric current density ($\bar{J}$) to electric field strength ($\bar{E}$), quantifying the material's electrical conductivity ($\tilde{\sigma}$) and its ability to conduct free charges under an electric field. Equation 5 connects electric displacement field ($\bar{D}$) to electric field strength ($\bar{E}$) through dielectric permittivity ($\tilde{\varepsilon}$), representing the displacement of charges in response to an electric field. Equation 6 describes the relationship between magnetic flux density ($\bar{B}$) and magnetic field intensity ($\bar{H}$) through magnetic permeability ($\tilde{\mu}$), capturing how atoms and molecules respond to a magnetic field.

Understanding these equations at the electromagnetic level empowers researchers and practitioners to analyze material responses to EM fields and enhance the capabilities of GPR technology. In GPR applications, assuming a scalar constant form for $\tilde{\sigma}$, $\tilde{\varepsilon}$, and $\tilde{\mu}$ is generally sufficient, with $\tilde{\varepsilon}$

and $\tilde{\sigma}$ being the most significant parameters of interest. This understanding forms the foundation for GPR scan analysis and aids in harnessing electromagnetic wave fields for effective material characterization.

Dielectric permittivity is a diagnostic physical property which characterizes the degree of electrical polarization a material experiences under the influence of an external electric field. Dielectric permittivity is the primary diagnostic physical property in GPR.

The dielectric constant, also known as the relative permittivity, ε_r, of a homogeneous media relates the relative EM velocity in a material to the speed of light in free space, c (Topp. et al 1980).

$$\varepsilon_r = (c/v)^2 \tag{2-7}$$

where, c = speed of light in free space of $3*10^8$ m/s.

2.5.3. GPR Electromagnetic mixing theories

In most GPR applications, variations in dielectric permittivity (ε) and electrical conductivity (σ) take precedence, while concerns about magnetic permeability (μ) are relatively rare. GPR proves highly effective when applied to low-electrical-loss materials, as in scenarios where σ approaches zero, the technology's versatility increases significantly, enabling signals to penetrate to greater depths. Nonetheless, such ideal low-electrical-loss conditions are infrequently encountered in real-world settings.

The real challenge arises from the fact that earth materials are inherently complex mixtures, comprised of various components. While certain substances like water and ice may consist primarily of a single component, materials such as simple beach sand are characterized by a combination of soil grains, air, water, and dissolved ions. Among these, soil grains tend to occupy a significant proportion, approximately 60-80% of the total volume. Effectively interpreting GPR

responses thus hinges on a comprehensive understanding of the physical properties exhibited by such mixtures.

However, material mixtures rarely demonstrate properties that directly correlate with the volume fraction of their individual constituents, introducing complexities in the quantitative analysis of GPR data. As a result, the interpretation process often necessitates the integration of additional ancillary information to achieve accurate and insightful assessments.

Key wave field properties in GPR include velocity (v), attenuation (α), and electromagnetic impedance (Z). These properties are most easily expressed when considering a simple medium with fixed permittivity, conductivity, and permeability and assuming a sinusoidal time variation with frequency (f) denoted by $\omega = 2\pi f$.

All wave properties exhibit similar behavior, with low frequencies showing a dependence on $\sqrt{\omega}$, indicating diffusive field behavior. In contrast, at high frequencies, the properties become frequency-independent, if electrical conductivity (σ), dielectric permittivity (ε), and magnetic permeability (μ) are also frequency-independent. The high-frequency behavior is particularly significant for GPR applications.

Conceptually, GPR systems are straightforward, aiming to measure field amplitude versus time after excitation. The core component of a GPR system is the timing unit, responsible for controlling signal generation and detection, understanding the wave field properties in GPR is crucial for interpreting data accurately and ensuring the effective functioning of the radar system during pavement inspections and evaluations.

The primary objective of reflection surveys in Ground Penetrating Radar (GPR) is to map subsurface reflectivity concerning spatial position. Variations in reflection amplitude and time

delay provide valuable information about the wave field properties, (ν), (α), and (Z). These surveys are traditionally conducted along straight survey lines, as GPR systems are designed to operate in this manner.

In essence, permittivity describes a material's ability to store and release electromagnetic (EM) energy in the form of electric charge. It can be likened to the storage capacity of capacitors. Alternatively, permittivity can be understood as a material's ability to restrict the flow of free charges or its degree of polarization (measured in F/m) under the influence of an applied electric field. The relative permittivity term (ε_r) is commonly used to express permittivity, denoting a nondimensional value. where:

$$\varepsilon_r = \frac{\text{permittivity of the material } (\varepsilon)}{\text{permittivity of free space or vacuum } (\varepsilon_o)} \tag{2-8}$$

The permittivity of free space, also known as the permittivity constant, is approximately 8.8542×10^{-12} F/m and is nearly identical to the permittivity of air. In the past, the relative permittivity of a material was sometimes referred to as the 'dielectric constant' and represented by the symbol κ, but this terminology is less common nowadays.

The permittivity of earth materials can vary significantly, particularly in the presence of free and bound water. It is a complex and frequency-dependent quantity, exhibiting both real (storage) and imaginary (loss) components. However, for practical purposes, the permittivity value of a material is often simplified to its constant, low-frequency (or static) real component, with the loss term disregarded. While this simplification is convenient for approximating radar wave velocities and wavelengths, it may not provide sufficient accuracy for detailed analysis.

Various formulations are practically useful for determining the effective permittivity of mixtures based on their constituent components. These formulations are generally designed for multi-phase mixtures composed of geometrically simple shapes or inclusions within a matrix. Examples include solid spheres in a fluid or uniform layers in a composite.

Several applicable formulations are available, including the Complex Refractive Index Model (CRIM), Maxwell-Garnet Theory (MGT), Effective Medium Theory (EMT), Looyenga Model, and Hanai-Bruggeman and Bruggeman-Hanai-Sen (BHS) models.

Among these formulations, the CRIM and its derivatives, as well as the BHS model, have gained popularity in GPR-based hydrological and contaminant applications. These models are favored for their simplicity, robustness, and accuracy across the GPR frequency range.

The Complex Refractive Index Model is specifically tailored for one-dimensional, layered medium scenarios. It has demonstrated effectiveness in cases involving medium-to-coarse grained, multi-phase mixtures with simple granular materials (e.g., semi-spherical sand grains) and moderate-to-low viscosity fluids.

The Complex Refractive Index Model (CRIM) offers the advantage of being a volumetric model, making it efficient in determining the effective permittivity of mixtures. This model only requires information about the permittivity of the constituent materials and their fractional volume percentages. Additionally, it can be applied to both the real and imaginary components of the complex permittivity.

In its general form, the CRIM formula is expressed as follows:

$$\varepsilon_{mix}{}^{e} = \left(\sum_{i=1}^{N} f \sqrt{\varepsilon_i}\right)^2 \tag{2-9}$$

$\varepsilon_{mix}{}^{e}$: complex bulk effective permittivity of the mixture

f : volume fraction of the ith component

ε_i : complex permittivity of the i^{th} component.

Saarenketo (1997) was among the pioneers in Europe to utilize GPR for measuring asphalt pavement density. His study was based on the concept that the dielectric constant of a pavement could be considered a function of the dielectric constants of its components. By recording the overall dielectric constants of the pavement, changes in the proportions of its constituents, such as void content, could be measured. The components of an asphalt mixture include asphalt, aggregate, air, and potentially water. Asphalt typically exhibits dielectric constants in the range of 3 to 6, crushed dry aggregate varies between 4.5 and 6.5, and air stands at 1.

Al-Qadi et al. (2010) expanded on this concept by developing three Hot Mix Asphalt (HMA) bulk specific gravity models based on the EM mixing theory. Through laboratory and field testing, they selected the most suitable model. They investigated the capability of GPR to predict in-place HMA density. The estimated HMA dielectric constant derived from GPR data allows the determination of its density and air void content when employing an appropriate model. Consequently, GPR can provide the density profile of the entire pavement, significantly improving the reliability of in-situ pavement density prediction, as other in-place density measurement methods only provide discrete sampling data.

Soil, being a composite material comprising solid particles, air, and water, has its density influenced by the specific gravities and volumetric fractions of its components. Similarly, the dielectric constant of soil is influenced by the dielectric and volumetric properties of its components, as previously mentioned. To predict the dielectric constant of soil mixtures, various EM mixing models are available, which are based on the dielectric constants and volume fractions

of the individual components. These models often assume a mixture composed of a background material with inclusions of different sizes and shapes.

2.5.4. GPR Interpolations

The most important factors in determining a soil's dielectric permittivity are porosity and water saturation. Air has a relative permittivity of 1.0 whereas common soil forming minerals have much higher relative permittivity. This means that for dry samples, the soil's bulk dielectric permittivity decreases as the porosity increases.

Figure 3 shows a schematic diagram of the reflections of a GPR signal from a layered pavement system.

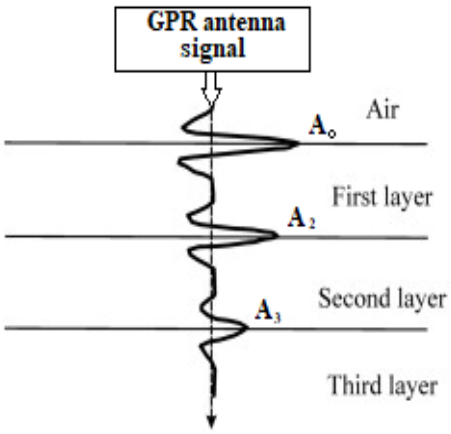

Figure 3. Multi layered system GPR signal reflection.

The dielectric values of the asphalt concrete (first layer) and the base layers can be computed using the following Eqs. (2-10) and (2-11), respectively.

$$\varepsilon_1 = \left(\frac{1 + \frac{A_0}{A_m}}{1 - \frac{A_0}{A_m}} \right)^2 \tag{2-10}$$

$$\varepsilon_{Base} = \varepsilon_{HMA}\left(\frac{1-\left(\frac{A_0}{A_m}\right)^2+\left(\frac{A_{Base}}{A_m}\right)}{1+\left(\frac{A_0}{A_m}\right)^2-\left(\frac{A_{Base}}{A_m}\right)}\right)^2 \quad (2\text{-}11)$$

ε_{HMA} = dielectric constant for the HMA layer,

A_o = amplitude of the surface reflection, and

A_m = amplitude of the reflected signal collected over a metal plate placed on the surface.

A_{base} = amplitude of the reflected signal collected over subbase layer surface.

The dielectric value ε_n for the third layer onwards (n^{th} layer) can be evaluated as Eq. (2-12), where γ_i is the reflection coefficient at the i^{th} layer interface calculated from Eq.(2-13)

$$\varepsilon_{r,n} = \varepsilon_{r,n-1}\left(\frac{1-\left(\frac{A_0}{A_m}\right)^2+\sum_{i=1}^{n-2}\gamma_i\left(\frac{A_i}{A_m}\right)+\left(\frac{A_n}{A_m}\right)}{1-\left(\frac{A_0}{A_m}\right)^2+\sum_{i=1}^{n-2}\gamma_i\left(\frac{A_i}{A_m}\right)-\left(\frac{A_n}{A_m}\right)}\right)^2 \quad n>2 \quad (2\text{-}12)$$

$$\gamma_i = \frac{\sqrt{\varepsilon_{r,i}}-\sqrt{\varepsilon_{r,i+1}}}{\sqrt{\varepsilon_{r,i}}+\sqrt{\varepsilon_{r,i+1}}} \quad (2\text{-}13)$$

Often a single calibration value (for determining material properties such as depth) is used for large amounts of collected GPR data, but currently there is usually very little analysis of how the calibration may be affected by variation in material properties within a pavement investigation site. The nature of materials at a site can be variable or may change, and in such circumstances, it may mean that data calibration procedures need to be altered to maintain the robustness of the information determined from GPR data. This issue not only relates to the effect of the material properties on the GPR data collected but also to the ability to quantify the levels of uncertainty or error in reported information.

2.5.5. Ground vs Air coupled antennas

GPR is commonly used to assess asphalt pavements, with two main types of GPR systems: air-coupled and ground-coupled. Air-coupled systems operate without direct pavement contact, making them faster and suitable for initial scanning to identify areas needing more detailed testing with ground-coupled GPR. Ground-coupled systems, requiring surface contact, offer superior depth penetration and provide more readings, making them ideal for comprehensive data collection and defining subsurface interfaces. Figure 4 illustrates examples of both ground-coupled and air-coupled antennas, which play a crucial role in obtaining accurate GPR data for assessing the condition of multilayer roadways.

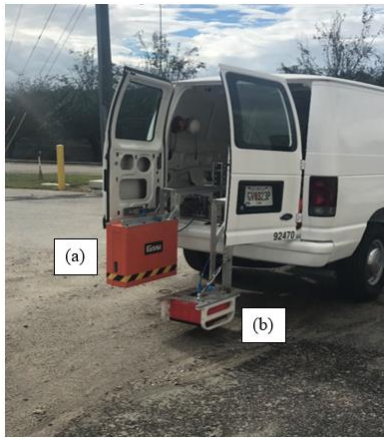

Figure 4 (a) GSSI 2 GHz air coupled antenna, (b) GSSI 400 MHz ground-coupled antenna

Both systems employ electromagnetic wave pulses within a frequency range of 100–5,000 MHz, capturing reflections from layer interfaces or other reflectors within the pavement (Vilbig, R. A., 2013). Reflections from the pavement surface and subsequent interfaces are analyzed to estimate the thickness of different pavement layers. Air-coupled GPR relies on non-contact sensing (Figure 5-a), while ground-coupled GPR operates with direct surface contact (Figure 5-b).

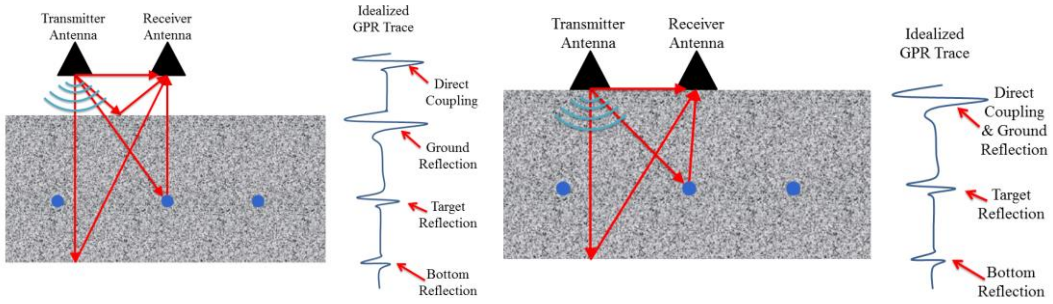

Figure 5 (a) air coupled antenna, (b) ground-coupled antenna

Ground-coupled antennas are advantageous when exploring deeper layers and thicker pavements, or when information about the pavement foundation is needed. In contrast, air-coupled horn antennas excel in high scan and data acquisition rates, facilitating faster surveys and enabling detailed assessment of surface conditions.

For pavement layer inspections, air-coupled horn antennas offer evident advantages. Their non-contact operation enables efficient and rapid data collection, reducing survey time and enhancing productivity. Additionally, the higher scan rates provide comprehensive evaluations of surface conditions, leading to more accurate pavement assessments. The choice between ground-coupled and air-coupled antennas depends on the specific objectives of the pavement inspection, considering the desired depth of analysis and the importance of surface conditions in the evaluation process.

2.6. AI APPLICATIONS IN PAVEMENT ENGINEERING

Artificial intelligence (AI) has found various applications in the field of pavement engineering, particularly in the area of automated distress detection and crack detection. Deep learning, specifically deep convolutional neural networks (CNNs), has emerged as a popular choice for computer vision-based automated pavement distress detection (Gopalakrishnan, 2018). These deep learning algorithms have shown groundbreaking achievements in other areas such as machine

translation, speech recognition, and computer vision, which has sparked interest in their application to pavement image analysis (Gopalakrishnan, 2018). Pavement crack detection using computer vision techniques has been widely studied but has faced limitations in real-world situations due to changes in lighting conditions and variation in textures (Pauly et al., 2017). However, recent advancements in artificial neural networks, especially in deep learning, have initiated new possibilities for applying computer vision methods to pavement crack detection (Pauly et al., 2017, Abdelmawla et al., 2023).

In fact, studies have shown that deeper networks in computer vision-based pavement crack detection can lead to improved accuracy (Pauly et al., 2017). In addition to crack detection, AI has also been applied to other aspects of pavement engineering.

For example, machine learning algorithms such as support vector machines, artificial neural networks, and random forests have been used to analyze multispectral pavement images acquired by unmanned aerial vehicles (UAVs) for distinguishing between normal pavement and pavement damages like cracks and potholes (Pan et al., 2018). This UAV remote sensing system offers a new tool for monitoring asphalt road pavement condition and can be used as decision support for road maintenance practices (Pan et al., 2018). Artificial neural networks have also been utilized in pavement management systems (PMS) for estimating current and predicting future pavement conditions, assessing maintenance needs, and selecting maintenance strategies (Domitrović et al., 2018). These neural networks can solve nonlinear engineering problems, including prediction and estimation, pattern recognition, and optimization (Domitrović et al., 2018).

By using artificial neural networks, it is possible to evaluate the existing pavement condition and define the maintenance strategy of national roads (Domitrović et al., 2018). Overall, AI, particularly deep learning and artificial neural networks, has shown great potential in various

applications within pavement engineering. These technologies can automate distress detection, improve crack detection accuracy, and assist in pavement management systems for better maintenance strategies. However, there are still challenges to overcome, such as variations in training and testing datasets and the depth of the neural networks used (Pauly et al., 2017). Further research is needed to address these challenges and explore the full potential of AI in pavement engineering (Gopalakrishnan, 2018).

2.6.1. Machine Learning in Pavement Assessment

Machine learning (ML) algorithms offer more efficient and precise pavement assessment than traditional methods. With the use of these algorithms, the assessment process becomes more automated, with the ability to predict pavement distress scores and detect asphalt conditions. Moreover, the integration of different data collection methods and cost-effective pavement monitoring strategies further enhances the capabilities of machine learning algorithms for pavement assessment. The results of these studies demonstrate the potential of machine learning in improving pavement assessment and maintenance. Therefore, it is important to continue exploring and developing these technologies to improve pavement performance and safety.

ML algorithms are gaining popularity in pavement assessment. Researchers have devised models that utilize automated pavement survey (APS) data, such as Laser Crack Measurement System, and traditional windshield pavement survey (WPS) data to predict pavement distress scores (Bai et al. 2023). Various machine learning algorithms, including Support Vector Machine, Random Forest, Naïve Bayes, Artificial Neural Networks, and Convolutional Neural Networks, have been employed to detect asphalt conditions using different data collection methods like images, ground penetrating radar (GPR), laser, and optic fiber (Cano-Ortiz et al. 2022). Furthermore, ML algorithms have been evaluated for predicting pavement serviceability, with techniques like

support vector machine, random forest, and artificial neural network exhibiting high accuracy (Luisa et al. 2023).

In addition, a cost-effective strategy for pavement monitoring has been developed by utilizing unsupervised machine learning algorithms and smartphone sensors, enabling daily pavement surface condition evaluation (Kyriakou and Christodoulou 2022). Furthermore, machine learning models have been used to assess the behavioral variations between human-driven vehicles (HDV) and connected and automated vehicles (CAV) in terms of pavement performance, with CAVs causing faster pavement deterioration than HDVs (Chen et al 2023).

2.6.2. Deep learning in pavement condition assessment

In recent years, the application of deep learning techniques in pavement condition assessment has garnered significant attention within the research community. One noteworthy study, cited as (Bai et al., 2023), introduced a deep learning framework specifically tailored for the automated evaluation of rural road pavement conditions. This innovative approach leveraged digital images captured from a dashboard-mounted camera to rate the pavement's condition accurately.

Another notable contribution, the research done by (Cano-Ortiz et al., 2022), proposed an advanced connected vehicle-based system harnessing deep learning algorithms to provide real-time predictions of slippery pavement conditions. This system holds promise for enhancing road safety by promptly alerting drivers to potentially hazardous situations.

Furthermore, a research endeavor, researchers in (Luisa et al., 2023), involved the development of a convolutional neural network (CNN) model capable of processing aerial images and generating estimations of pavement condition indices. This application showcases the versatility of deep learning techniques in handling diverse data sources for pavement assessment.

Moreover, a comprehensive review publication, (Kyriakou and Christodoulou, 2022), conducted an in-depth examination of various methods for recognizing pavement conditions. Additionally, it introduced a measurement system that harnesses machine learning methods to effectively determine pavement condition, underscoring the adaptability of these techniques in the field.

Lastly, an investigation, referred to (Chen et al., 2023), explored the feasibility of modeling and predicting pavement distress across multiple lanes. This study employed a combination of multiple linear regression analysis and artificial neural networks, demonstrating the potential of deep learning in advancing the accuracy and scope of pavement condition assessment.

These studies collectively show the significant potential of deep learning approaches in the continual improvement of pavement condition assessment methodologies.

2.6.3. GPR data analysis using deep learning.

Numerous investigations have delved into the application of deep learning techniques to analyze GPR data for pavement assessment and distress detection. One study, performed by (Bashar et al. 2022), introduced an innovative method that combines object detection algorithms with GPR images to identify concealed cracks within asphalt pavement. In another study, (Chen et al. 2022) proposed the use of the deep learning-based object detection algorithm, Mask R-CNN, for the automatic identification of road void distress from GPR images. Moreover, a study, run by (Liu 2022), centered on employing GAN models to enhance pavement texture data and thereby improve the classification accuracy of deep learning models for pavement texture recognition. These investigations and others collectively highlight the potential of deep learning techniques in the analysis of GPR data for pavement assessment and distress detection. It is evident that the integration between deep learning and GPR data holds promise for enhancing the precision of pavement analysis and distress detection. Future research in this domain could explore the

application of more intricate deep learning models and larger datasets to further bolster the effectiveness of pavement analysis through GPR data or further by using satellite images.

2.7. ADVANCEMENTS IN PAVEMENT DISTRESS PREDICTION

Significant progress has been achieved in the realm of pavement distress detection by leveraging the capabilities of machine learning algorithms and deep learning-based image segmentation models. These methodologies offer expedited, automated, and intelligent means to identify and evaluate pavement distress, including issues like cracks and potholes (Gao et al. 2023 & Wu and Jin 2023). The application of unsupervised learning techniques has played a pivotal role in extracting highly correlated factors and effectively segregating attributes that define pavement functional performance. This, in turn, facilitates the selection of appropriate preventive maintenance strategies (Yi et al. 2023).

Furthermore, the utilization of multi-sensor systems, exemplified by the Azure Kinect, has emerged as a valuable tool for gathering pavement distress data, even under challenging low-light nighttime conditions. This not only enhances the accuracy of distress segmentation but also enables a more comprehensive assessment of distress severity (Sandamal et al. 2023). In parallel, the integration of explainable and supervised machine learning algorithms has proven instrumental in predicting road roughness, furnishing both precise forecasts and transparent rationales for decision-making processes (Deng and Tan 2023).

These advancements represent crucial strides in the field of pavement distress detection, contributing to the formulation of cost-effective and sustainable strategies for pavement maintenance and rehabilitation

CHAPTER 3

DENSITY PREDICTION MODEL

Road construction projects demand rigorous quality control processes to ensure the resiliency and sustainability of infrastructure. A critical aspect of this quality control is the assessment of soil density in subgrade and base materials. Traditional methods, such as the sand cone test, SPT field test and nuclear gauge density test have long been employed for this purpose. However, GPR technology presents an opportunity to revolutionize this practice.

This chapter unveils the development and practical implementation of the GPR-Density prediction model—a pioneering approach to soil density assessment in road construction. In this chapter, the possibility to infer the physical characteristics of unbound compacted subgrade soils from their dielectric properties through GPR is investigated. Specifically, this study is aimed at providing a GPR-based approach for an effective and efficient pavement assessment model. The proposed model was calibrated through laboratory tests conducted under controlled compaction conditions and validated by using in situ density measurements.

3.1. GPR-DENSITY MODEL DERIVATION

GPR is a powerful tool used in geophysical investigations, and it has shown great promise in understanding current condition for various civil engineering applications. The core concept behind this model lies in the analysis of GPR data, which provides valuable insights into subsurface conditions.

The derivation of the GPR-Density model can be divided into several key steps. As a start, an exploration of the fundamental principles that underpin GPR technology and its interaction with different soil types is done. From there, the mathematical framework that transforms GPR data into meaningful density predictions takes place.

Based on previously mentioned theories in Chapter 2, it could be concluded that soil dry density, water content and porosity could be attributed to the value of dielectric constant and subsequently could be estimated based on its value.

In accordance with the CRIM mixture theory, the dielectric constant of a homogenous mixture can be estimated by the "power-law" approximation. A widely used class of mixing models is shown in equation (3-1).

$$\varepsilon_{eff}^{\beta} = f\,\varepsilon_{i}^{\beta} + (1-f)\,\varepsilon_{e}^{\beta} \tag{3-1}$$

In this mixing model, a certain power of the permittivity is averaged by volume weights. f is the volume fraction and b is a constant dependent on the mixture's composition and is usually assumed to be 0.5 (Sihvola, 1999). Soil is a composite material that consists of solid particles, air, and water. Density of soil depends on the specific gravities and volumetric fractions of its components. In a similar way, the dielectric constant of the soil is a function of the dielectric and volumetric properties of its components as previously mentioned.

Assuming the total volume of soils phases is assumed as 1, Eq (3-1) can be re-written as Eq (3-2).

$$\varepsilon_{soil}{}^{\beta} = V_a.\varepsilon_a{}^{\beta} + V_w.\varepsilon_w{}^{\beta} + V_s.\varepsilon_s{}^{\beta} \tag{3-2}$$

It could be concluded that soil density, water content and porosity could be attributed to the value of dielectric constant and subsequently could be estimated based on its value.

Accordingly, after that a model is proposed through this research to estimate both mass water content and soil dry density, using dielectric constant calculated depending on field or lab measurements of GPR. Using previous perspective and depending on equation (3-2) and soil phase diagram the model could be derived as follows.

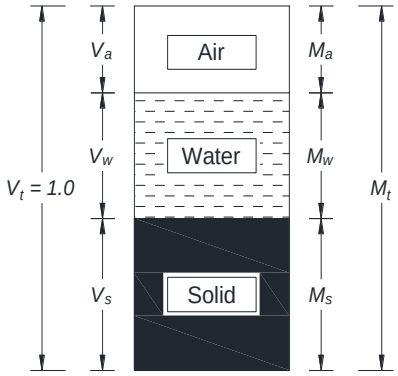

Figure 6. Soil phase diagram

V_a : air voids volume in soil , M_a : air voids mass = 0

V_w : water volume in soil , M_w : mass of water

V_s : solid particles volume in soil , M_s : mass of solids

ε_{soil} : soil media dielectric constant , ε_a : air dielectric constant = 1.0

ε_w : water dielectric constant = 80-81 , ε_s : soil particles dielectric constant

From Phase diagram relations, Assuming $V_t = 1.0$

$\because \gamma_d = \frac{GS.\gamma_w.(1-\frac{V_a}{V_t})}{1+w.GS} = \frac{GS.\gamma_w.(1-V_a)}{1+w.GS}$, $\therefore V_a = 1 - \frac{\gamma_d.(1+w.GS)}{GS}$ --------- (i)

$\because \gamma_d = \frac{M_S}{V_t} = M_S$, $\therefore \gamma_d = M_S$ --------- (ii)

$V_w = w.M_S$ --------- (iii), $V_s = \frac{M_S}{GS}$ --------- (iv)

$\varepsilon_{soil}{}^{0.5} = V_a.\varepsilon_a{}^{1/\alpha} + V_w.\varepsilon_w{}^{0.5} + V_s.\varepsilon_s{}^{0.5}$ --------- (v)

Substituting i, ii, iii and iv in v

$$\therefore \sqrt{\varepsilon_{soil}} = 1 - \frac{\gamma_d.(1+w.GS)}{GS} + w.\gamma_d.\sqrt{\varepsilon_w} + \frac{\gamma_d}{GS}.\sqrt{\varepsilon_s}$$

$$\therefore \sqrt{\varepsilon_{soil}} - 1 = \gamma_d.\left[-\frac{1}{GS} - w + w.\sqrt{\varepsilon_w} + \frac{1}{GS}.\sqrt{\varepsilon_s}\right]$$

$$\therefore \sqrt{\varepsilon_{soil}} - 1 = \gamma_d.\left[\frac{1}{GS}\left(\sqrt{\varepsilon_s} - 1\right) + w\left(\sqrt{\varepsilon_w} - 1\right)\right]$$

$$\therefore \gamma_d = \frac{\left(\sqrt{\varepsilon_{soil}}-1\right)}{\frac{1}{GS}\left(\sqrt{\varepsilon_s}-1\right)+w\ \left(\sqrt{\varepsilon_w}-1\right)} \quad (3\text{-}3)$$

Note that in these equations, the specific gravity of a material is equal to the density of the material divided by the density of water at 4° C (1g/cm^3), and therefore is numerically the same as the density of the material in g/cm^3.

Topp et al. (1988) proposed equation (3-4) to estimate the volumetric water content (θ) in relation with dielectric constant of the soil. The water content of soil is calculated from volumetric water content as shown in equation (3-5).

$$\theta = -0.053 + 0.0292\ (\varepsilon_{soil}) - 5.5\text{x}10^{-4}\ (\varepsilon_{soil})^2 + 4.3\text{x}10^{-6}\ (\varepsilon_{soil})^3, \quad (3\text{-}4)$$

$$w = \theta\ /\ \gamma_{soil} \quad (3\text{-}5)$$

3.2. MODEL IMPLEMENTATION

In this section, an outline that represent the step-by-step implementation process of the GPR-Density model for estimating soil dry density is presented. The process involves calculating the gravimetric water content (w) and subsequently deriving the corrected dry density of the subgrade layer.

Step 1: Initial Gravimetric Water Content (w_i): The first step is assuming a gravimetric water content as a starting point, followed by calculation of initial density.

Step 2: Volumetric Water Content Calculation (θ): calculation of the volumetric water content (θ) using Equation (3-4). This initial calculation provides the value for water content based on GPR data and the model's mathematical framework.

Step 3: Gravimetric Water Content Calculation (w): next, the volumetric water content (θ) is converted into gravimetric water content (w) using Equation (3-5) and initially calculated dry density as per the guidelines provided by AASHTO. This step is essential to facilitate the subsequent error correction process.

Step 4: Error determination and minimization with GRG: With both the calculated gravimetric water content (w) and assumed gravimetric water content (w_i) in hand, the model proceeds to determine the error between these values. The error calculation highlights any disparities between the model's assumptions and the actual soil conditions. To rectify the errors identified in the previous step, the Generalized Reduced Gradient (GRG) optimization technique is employed. GRG is utilized to minimize the error until reaching a value of (0.001), and iteratively adjust the assumed values for gravimetric water content (w) until a more accurate estimation is achieved.

Step 5: Recalculation of Corrected Dry Density: after minimizing the error and obtaining corrected values for gravimetric water content (w), the model recalculates the corrected dry density of the subgrade layer using Equation (3-4). This final step yields a more precise estimation of dry density based on the corrected water content values.

Figure 7 illustrates the entire process, from the initial assumption of water content to the final determination of corrected dry density.

By following these structured steps, the GPR-Density model ensures a robust and accurate estimation of soil dry density. The incorporation of error determination and correction mechanisms, including the use of GRG optimization, enhances the model's reliability for civil engineering applications.

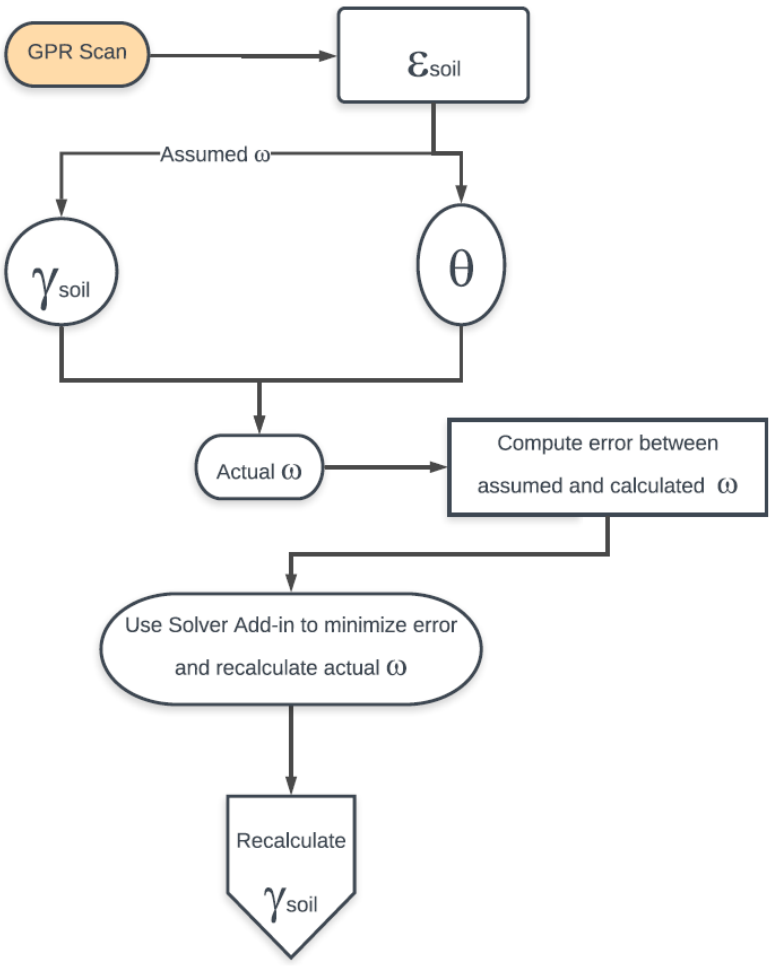

Figure 7 GPR-Density model implementation

3.3. MODEL CALIBRATION IN LABORATORY

The subgrade density model, as represented by Equation 3-3, underwent a thorough calibration process through a series of rigorous laboratory and field tests. This calibration aimed to refine and enhance the model's precision in estimating subgrade soil properties. The subsequent sections offer a comprehensive insight into the meticulous steps taken during this calibration procedure.

A set of laboratory tests were conducted to build the database to prove the proposed method in establishing the relationship between GPR scanning results and subgrade soil physical properties. The laboratory testing program took place at the University of Georgia's (UGA) Geomaterials

Research Lab in Athens, Georgia. A problematic high plastic silt soil readily found in North Georgia was used as the subgrade material. Test specimens were prepared in a large metal box measuring 2 m long × 2 m wide × 0.7 m deep (6 ft long × 6 ft wide × 2 ft deep), as shown in Figure 8. Each sample measures 1.0 m long × 0.7 m wide. The soil and water were mixed till reaching the desired water content for soil compaction. The soil was then transported to the steel box and gradually compacted using a vibrating table. GPR surveys were carried out for each compaction step up to the maximum density available, as shown in Figure 8. Subgrade soil specimens were constructed with 0.3 m (12 inches) in depth and compacted to reach six different density levels, as shown in Figure 9.

The physical properties of the soils were measured to compare the properties derived from the GPR scan results.

Figure 8 Sample preparation photos: (a) Soil transportation and filling testing box, (b) soil compaction

Figure 9 divided soil samples

3.3.1. Grain size Distribution

The soil was classified as high plasticity silt (MH) per the Unified Soil Classification System (USCS) and A-7-5 according to the AASHTO classification system.

3.3.2. Specific Gravity

The specific gravity of the tested soil was calculated based on ASTM D854-14. The specific gravity value is vital for GPR–density model calculations. The soil index properties for these soils are provided in Table 1.

Table 1 Soil specimen index properties.

Specific Gravity	USCS Classification	Fines (%)	PL	LL	PI
2.76	MH	57.21	37.44	57.1	19.7

3.3.3. Maximum Dry Density

The maximum dry density for the soil sample was measured in accordance with ASTM standard D1557. The soil maximum dry density was found to be 116.75 pcf (1.871 t/m^3) with optimum water content of 24.6 percent.

3.3.4. Laboratory Sand Cone Test

After the specimens were prepared, the bulk density of each specimen was measured using sand cone tests. The results of the sand cone tests are illustrated in Table 2.

Table 2 Lab sand cone test results

Sample	Bulk density (γ_{bulk})		Water content %	Dry density (γ_{dry})	
	(t/m^3)	(pcf)		(t/m^3)	(pcf)
D1	1.951	121.8	22.49%	1.593	99.4
D2	2.119	132.3	21.05%	1.750	109.3
D3	1.759	109.8	20.43%	1.461	91.2
D4	2.321	144.9	24.43%	1.865	116.4
D5	2.090	130.5	26.60%	1.651	103.1
D6	1.603	100.1	18.69%	1.351	84.3

It should be noted that specimens D1 through D5 were compacted with varying compaction efforts, while D6 was not compacted at all. Therefore, it is believed that the D6 specimen had a higher void ratio compared to the other specimens.

3.3.5. Laboratory GPR scan results

After the sand cone tests were conducted, GPR data were collected from six samples using a 2.0 GHz air-coupled antenna, as shown in Figure 10. The data acquisition system was calibrated before each scan to validate the signals with a perfect reflection on a metal plate. This calibration also provided some preliminary data for the processing, with A_m (amplitude of the reflected wave on the

metal plate to estimate the dielectric constants for the subsequent layers) to calculate the density and water content ratios for the targeted samples by the GPR scan.

Figure 10 GPR Scanning and calibration for different samples

The calibration of the GPR system was performed with a metal plate on top of the soil specimen. From this calibration process, A_m was found to be 7,942,173, as shown in Figure 10.

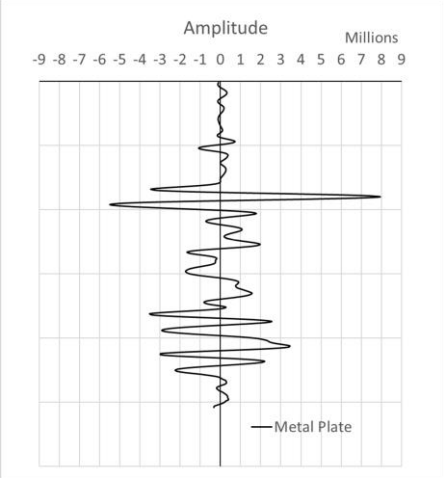

Figure 11 Amplitude from metal plate calibration

Figure 12 shows the amplitude of the surface reflection measured from each soil specimen. Using the measured amplitude values from GPR, the dielectric constants for the six soil specimens were

calculated using equation (2-10). Table 3 summarizes the calculated dielectric constant for each specimen.

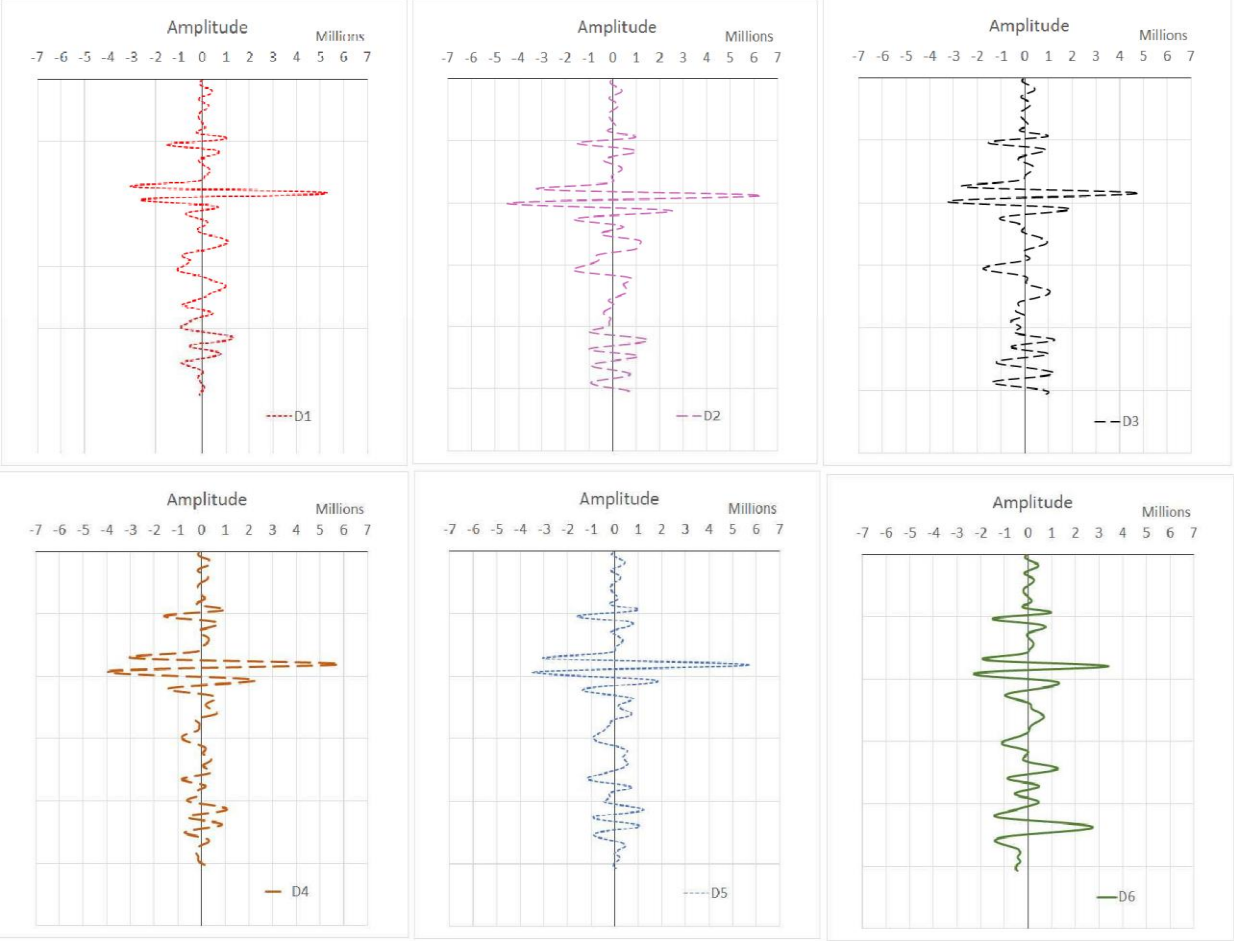

Figure 12 Amplitude for different soil samples

Utilizing the measured amplitude values obtained from the GPR scans, the dielectric constants (ε) for each of the six soil specimens are calculated. Table 3 summarizes the calculated dielectric constants.

Table 3 Dielectric constant results

Sample ID	Amplitude	ε
D1	5,257,634	24.18
D2	5,318,661	25.55
D3	4,827,136	16.80
D4	5,788,944	40.67
D5	5,740,596	38.63
D6	3,378,338	6.15

3.3.6. GPR-Density Model Calculations

The results from both laboratory sand cone tests and GPR scans were integrated into the GPR-Density model, which was subsequently used to estimate soil properties. Table 4 presents the outcomes of the model's calculations, including initial and corrected water content (w) and dry density (γ_{dry}):

Table 4 Proposed model calculation results*

Sample ID	w % Measured	γ_{dry} Initial		θ	w % Calculated	γ_{dry} Calculated	
		t/m^3	pcf			t/m^3	pcf
D1	22.5%	1.977	123.4	39%	17%	1.644	102.6
D2	21.1%	2.047	127.8	41%	17%	1.702	106.2
D3	20.4%	1.564	97.7	30%	17%	1.301	81.20
D4	24.4%	2.714	169.4	51%	16%	2.257	140.9
D5	26.6%	2.632	164.3	50%	16%	2.189	136.7
D6	18.7%	0.747	46.7	11%	13%	0.621	38.80

* ε_w = 80 (80-81), ε_s = 15 (5-30)

Table 5 shows the calculated dry density from the model and measured bulk density from the sand cone tests. Generally, the percentage error ranged from 3 to 24 percent. A substantial error of 118% was observed for the specimen with the lowest density. Figure 13 shows the comparison of measured and calculated dry densities along with the line of equality.

Table 5 Comparison between proposed model and sand cone test results

Sample ID	γ_{dry} Calc.		Dry Density (Sand Cone Test)		Error %
	t/m^3	pcf	t/m^3	pcf	
D1	1.637	102.2	1.593	99.4	3%
D2	1.695	105.8	1.750	109.3	3%
D3	1.295	80.9	1.461	91.2	13%
D4	2.247	140.3	1.865	116.4	17%
D5	2.180	136.1	1.651	103.1	24%
D6	0.619	38.6	1.351	84.3	118%

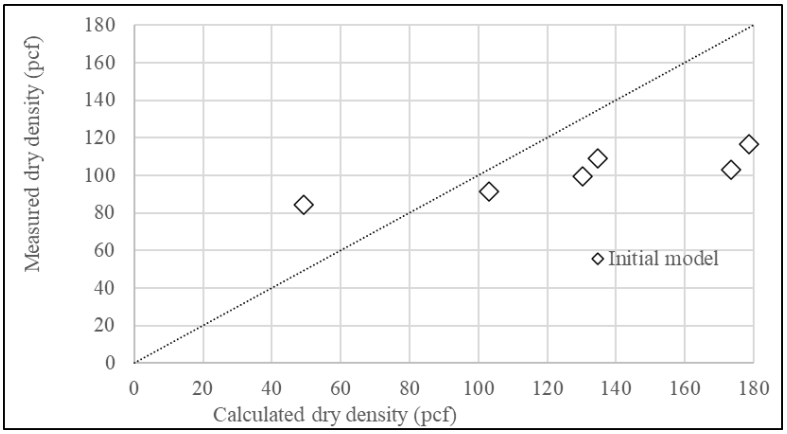

Figure 13 Comparison between measured and calculated soil dry densities

Abdelmawla and Kim (2020) proposed a model that measured density should be validated with a back calculated value to reflect the soil physical properties in the field. To adjust the error between the calculated and measured bulk density, an exponential model was utilized, as shown in equation.

$$\gamma_{dry,\ estimated} = \alpha\,(\gamma_{dry,\ calculated})^{\beta} \qquad (3\text{-}6)$$

Based on the laboratory tests, the fitting coefficients of a and b were estimated as 1.464 and 0.171, respectively. It should be noted that these fitting coefficients were developed for highly plastic silt

soils and should be used with caution for other soil types. The comparisons of measured and calculated subgrade density are shown in Table 6 and Figure 14.

Table 6 Exponential model results.

Sample ID	γ_{dry} Measured		γ_{dry} Calculated with fitting coefficients		% Error
	t/m^3	pcf	t/m^3	pcf	
D1	1.593	99.4	1.593	99.4	0%
D2	1.750	109.3	1.602	100.0	9%
D3	1.461	91.2	1.531	95.6	5%
D4	1.865	116.4	1.681	104.9	11%
D5	1.651	103.1	1.672	104.4	1%
D6	1.351	84.3	1.351	84.3	0%

The subgrade soils' dry density estimated by the new exponential model shows approximately 11 percent maximum error compared to the soil's density measured by the sand cone method.

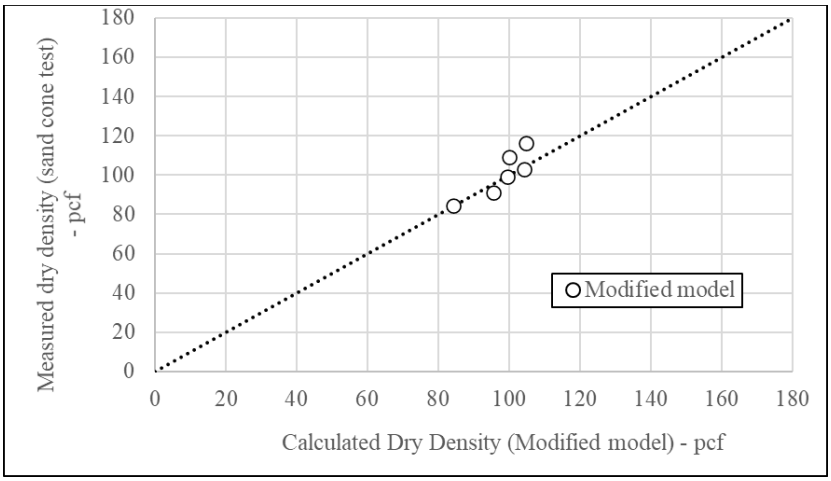

Figure 14 Exponential model vs measured soil bulk density

3.4. FIELD TEST VALIDATION

Utilizing the University of Georgia (UGA)'s dedicated GPR van, which is equipped with antennae mounted at the rear, facilitating the comprehensive scanning of road surfaces.

Field tests were conducted to validate the GPR–density model. Three sites were selected in the state of Georgia. Details of these locations on State Route (SR) 53, SR 81, and SR 316 are shown in Table 7 and depicted in Figure 15.

Table 7 Verification field tests

Site	Location				
	Start		End		Length (ft)
SR 53	34.417658	-84.304409	34.4175185	-84.3054911	352.57
SR 81	33.989741	-83.7787341	33.9912852	-83.7782494	626.52
SR 316	33.945245	-83.7518097	33.9447035	-83.7508741	350.10

(a) (b) (c)

Figure 15 Field verification (a) SR-53, (b) SR-81, (c) SR-316

GPR tests were carried out along two lines of scan across the lane width. The procedure was validated through sand cone tests to obtain field bulk density, dry density, and water content; results are shown in Table 8 for the three field test sites.

Table 8 SR 53 sand cone test results

State Route (SR)	Sample	Bulk Density (γ_{bulk})		Dry Density (γ_{dry})		Water Content (%)
		(t/m^3)	(pcf)	(t/m^3)	(pcf)	
SR-53	S1	1.925	120.2	1.823	113.8	5.6%
	S2	2.045	127.7	1.934	120.7	5.7%
SR-81	S1	2.162	135.0	1.729	107.9	23.7%
	S2	2.005	125.2	1.635	102.1	19.9%
	S3	2.087	130.3	1.696	105.9	24.2%
SR-316	S1	2.018	126.0	1.833	114.4	10.1%
	S2	1.936	120.9	1.764	110.1	9.8%

GPR frequency data were collected using the UGA GPR van; a GPR SIR-30 scan system was deployed with two different antennas at two different frequency levels, 2 GHz, and 400 MHz. The UGA GPR system installed in the van is custom built, as shown in Figure 16 and Figure 17.

Figure 16 UGA GPR van

Figure 17 UGA GPR road survey control units

3.5. VALIDATION TEST SUMMARY

Our field results provided valuable insights into the model's performance in estimating subgrade soil dry density. The model's estimates for SR 53 were compared to the outcomes of sand cone tests conducted on field samples, and the maximum error observed in the estimated results was 5 percent. This discrepancy is relatively small and falls within an acceptable range for subgrade density estimation as illustrated in Table 9. Figure 18 illustrates the calculated dry density for SR 53, indicating a consistent and reliable estimation throughout the road section. These field results indicate that the proposed model holds promise for accurately assessing subgrade soil properties on SR 53, which is essential for effective pavement performance evaluation and maintenance planning.

Table 9 Sand cone test results

State Route (SR)	Distance	γ_d Meas.		γ_d Calc.		Error
	ft	t/m^3	pcf	t/m^3	pcf	
SR-53	20.00	1.823	113.8	1.928	120.3	5%
	120.00	1.934	120.7	1.957	122.2	1%
SR-81	20.00	1.823	113.8	1.928	120.3	5%
	120.00	1.934	120.7	1.957	122.2	1%
SR-316	350.00	1.833	114.4	1.833	114.5	0.02%
	300.00	1.764	110.1	1.764	110.1	0.00%

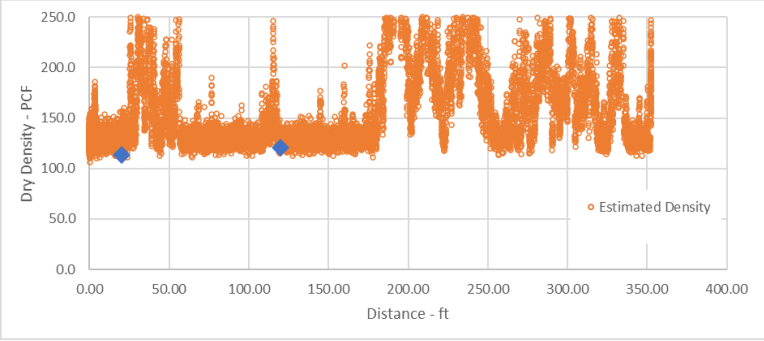

Figure 18 Calculated dry density for SR 53

Similarly, field results for SR 81 and SR 316 provided significant insights into the model's capabilities in estimating subgrade soil dry density. For SR 81, the model demonstrated a remarkably low error, with a maximum of only 0.02 percent when compared to sand cone test results as shown in Table 9. Figure 19 showcases the calculated dry density for SR 81, depicting the model's consistent and precise estimates along the road section. Additionally, Figure 20 for SR 316 demonstrates the model's ability to estimate subgrade density accurately, with a maximum error of 2.67 percent. These field results suggest that the proposed model can provide reliable estimates of subgrade soil properties for both SR 81 and SR 316. These findings have implications for identifying areas with potential pavement performance issues, ultimately contributing to more effective infrastructure maintenance and longevity.

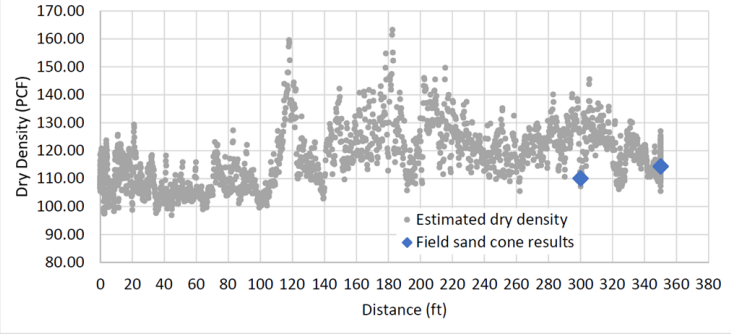

Figure 19 Calculated dry density for SR 81

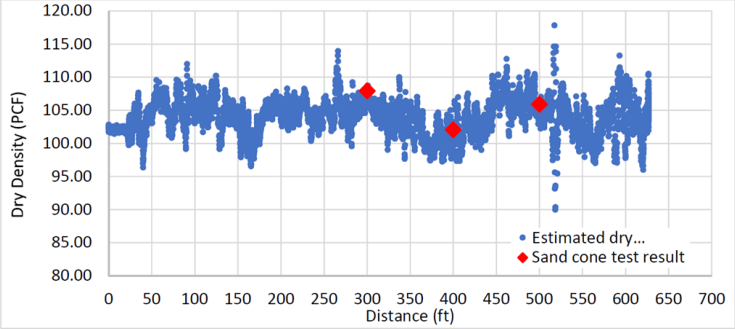

Figure 20 Calculated dry density for SR 316

3.6. MODEL APPLICATION CONCOLUSION

In conclusion, this phase of the research has successfully developed and validated a self-consistent method that leverages the analysis of GPR signals in the frequency domain to assess subsurface moisture and predict subgrade dry density. The application of this method holds great promise for a wide spectrum of nondestructive applications.

One of the key findings of this study is the feasibility of inferring subsurface moisture content through permittivity measurements obtained via GPR. This discovery underscores the potential of GPR technology as a valuable tool for assessing and monitoring subsurface moisture, which is critical in various applications.

Additionally, the proposed semi-empirical model for subgrade dry density prediction has proven to be effective, particularly for fine-grained soil types. While it tends to overestimate dry density for higher moisture levels, it exhibits greater accuracy when applied to low-moisture soils. This indicates that the model is particularly well-suited for estimating subgrade dry density in scenarios involving drier soil conditions.

Moreover, the research has unveiled a positive correlation between relative dielectric permittivity and density, highlighting that greater material compaction corresponds to higher relative permittivity. This relationship offers insights into how GPR technology can be employed to indirectly assess subgrade density in various applications.

The predictive accuracy of the proposed model is a noteworthy outcome, with an overall error rate of less than 11 percent in most surveyed stations. This level of precision underscores the practical utility of the model, especially in infrastructure assessment and maintenance planning.

Based on these findings, future research should exercise caution in GPR trace averaging, explore varied frequency ranges for GPR applications, and investigate the estimation of soil mechanical properties like strength and elasticity from GPR data. Additionally, emphasizing the significance of field validation, especially for network-level roads, is crucial to fully leverage GPR systems in assessing road infrastructure integrity.

CHAPTER 4

SUBSURFACE ANOMALY DETECTION

In pavement engineering, cracks represent a significant concern, often arising from material irregularities, internal stresses, and the effects of dynamic traffic and weather. These cracks, particularly the hidden internal ones known as bottom-up cracks, can compromise structural integrity and accelerate pavement deterioration. Detecting and assessing these cracks accurately is crucial for diagnosing damages and selecting appropriate repair strategies.

GPR technology has become a widely adopted non-destructive method for identifying subsurface anomalies, including pavement cracks. Modern GPR systems, equipped with air-coupled antennas mounted on vehicles, enable high-speed inspection of pavement subsurface conditions. However, the sheer volume of GPR scan data has made manual analysis impractical, necessitating the development of automated subsurface anomaly detection algorithms.

Recent research has shown the potential of characterizing the pavement cracking process, including the examination of crack structures, assessment of root depth, and diagnosis of structural integrity, even in complex scenarios beyond simple transverse cracks. Vertical crack responses, whether visible on the surface or not, are also observable in pavement, often appearing at joints or propagating from beneath granular materials due to water infiltration.

While GPR measurements have traditionally relied on human inspection, neural networks (NN) have been developed to automatically recognize target features in GPR images. However, NN-based methods have limitations, particularly in recognizing complex features and their generalization capabilities. Deep convolutional neural networks (CNNs) have emerged as a promising solution, offering hierarchical feature representation and location-invariant feature extraction.

4.1. METHODOLOGY

The methodology used in this research to detect subsurface anomalies, specifically focusing on the identification of subsurface cracks in pavement is explained in coming sections. Research approach combines the power of ground-penetrating radar (GPR) technology with deep learning techniques. Various key components of methodology include deep learning model, data acquisition and augmentation techniques, image annotation, model training, and the subsequent deep learning model experiment. Additionally, results and conclusions drawn from the research is discussed.

4.2. DEEP LEARNING MODEL

YOLOR (You Only Learn One Representation) stands out as a leading real-time object detection algorithm renowned for its exceptional speed and accuracy. Its widespread adoption across various object detection applications underscores its significance in the field of computer vision. YOLOR's innovative architecture introduces a unified network that encodes both explicit and implicit knowledge, mirroring the human brain's ability to acquire knowledge through conscious and subconscious learning processes. By integrating these two forms of knowledge, YOLOR achieves

a versatile representation that transcends specific tasks. This breakthrough not only maintains detection accuracy comparable to YOLOv4 but also significantly reduces inference time, establishing YOLOR as one of the premier choices for real-time object detection tasks.

The power of the YOLOR model is used to tackle the critical issue of subsurface crack detection in pavement. Specifically, the model is designed to identify distinct class of subsurface crack, which is bottom cracks. To maximize the model's performance and leverage the knowledge learned from diverse datasets, COCO — pretrained weights — a dataset encompassing a wide array of object categories is used to pretrain the model. Subsequently, fine-tuning the model using proprietary GPR scan image dataset, tailoring it to the intricacies of subsurface crack detection. This fusion of transfer learning and YOLOR's capabilities forms the cornerstone of this research, with the aim of enhancing infrastructure maintenance and safety through more efficient crack detection methodologies.

The utilization of YOLOR in this study represents a pivotal advancement in the field, as it empowers us to leverage the cutting-edge capabilities of a real-time object detection algorithm to address a specific and critical problem in pavement maintenance. This integration positions research at the intersection of deep learning and infrastructure management, offering a promising solution to the challenges posed by subsurface cracks in roadways.

4.3. DATA ACQUISITION AND AUGMENTATION TECHNIQUES

The GPR scan images employed in this study were meticulously collected from various road sections located in Atlanta and Athens, Georgia, USA, GPR Dataset.

The extensive data collection efforts yielded an abundant dataset, encompassing over 400 miles of road scans. However, it is noteworthy that the presence of target features, essential for training a YOLOR model for subsurface crack detection, was relatively scarce within the retrieved GPR images.

A total of 6,000 images were initially extracted from the GPR scan recordings. Subsequently, a screening process was executed to select 500 images bearing conspicuous features, which were then subjected to manual labeling. Representative examples of extracted GPR images are displayed in Figure 21. These images exhibit distinct irregularities that are indicative of subsurface cracks within the pavement structure.

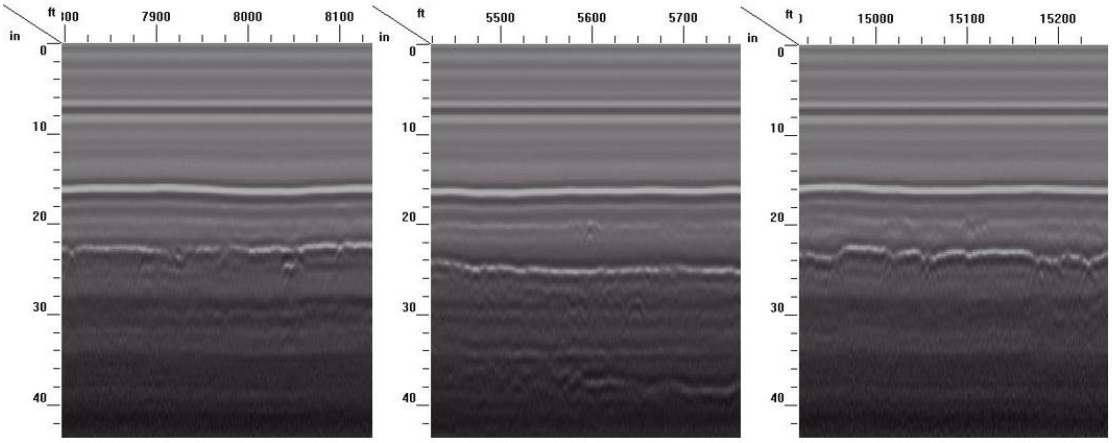

Figure 21 Extracted GPR images

Notably, these GPR images display unique features that signify internal cracks. Figure 22 illustrates examples of enlarged feature patches, representing two dominant crack types: bottom cracks and full cracks.

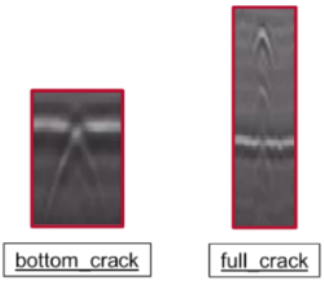

Figure 22 GPR features to be extracted

The distinctive features discernible in GPR scans, indicative of pavement cracks, have inspired adoption of deep learning-based object detection algorithms for their identification. The identification process hinges on the analysis of electromagnetic wave propagation velocity variations across pavement layers, with the presence of cracks and voids manifesting as inhomogeneities. These inhomogeneities are revealed through characteristic hyperbolic signatures or reflection patterns in the GPR image, with the amplitude and frequency of the reflected electromagnetic wave offering insights into the dimensions of the crack, including depth, length, and width.

To facilitate the effective detection of target features, it is imperative to perform image cropping, isolating the region of interest—the pavement layers exclusively. Figure 23 exemplifies the transition from raw GPR images to cropped images, wherein the algorithm's focus is concentrated on the pertinent region.

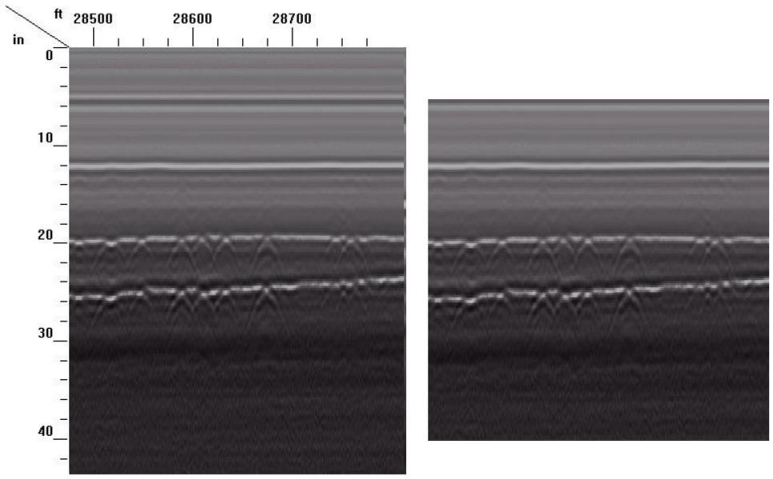

Figure 23 Image cropped to focus on pavement layers only

Once the images are appropriately cropped to encompass the region of interest, they undergo annotation to highlight target features. As a result, a total of 634 images underwent annotation, and the corresponding annotated target features are summarized in Table 10.

Table 10 GPR Scan Image Annotation

Class Label	# of Images	# of Labels
Bottom Crack	360	1929
Full Crack	274	329

Table 10 provides a summary of the GPR scan image annotation process, including the class labels, the number of annotated images, and the total number of labels for each class:

These class labels exclusively pertain to the presence or absence of bottom cracks or full cracks within each image, indicating their respective locations. It is pertinent to note that the images often encompass both types of cracks.

While the utilization of online labeling tools expedited the annotation process and improved efficiency, the manual labeling procedure was pivotal in upholding the accuracy and reliability of the dataset intended for the study.

Given the relatively limited number of annotated images available for model training, synthetic data generation becomes a crucial augmentation strategy to bolster the labeled dataset. The two data augmentation methods employed are discussed in the subsequent subsections.

To address the challenge posed by the scarcity of target features, two innovative augmentation methods are devised. These augmentation strategies were instrumental in augmenting the dataset, thereby facilitating the effective training of the YOLOR model.

The first augmentation method involves the generation of synthetic images by inserting target features into images that initially lack such features. This strategy leverages the wealth of unfeatured images available within the dataset. By inserting extracted target feature patches into these unfeatured images, new data is create synthetic data, as illustrated in Figure 24 (referred to as "Augmentation 1").

The second augmentation method capitalizes on the available featured images, those containing target features, to generate new featured images. This augmentation technique enhances the dataset by introducing variations of featured images, denoted as "Augmentation 2" in Figure 24.

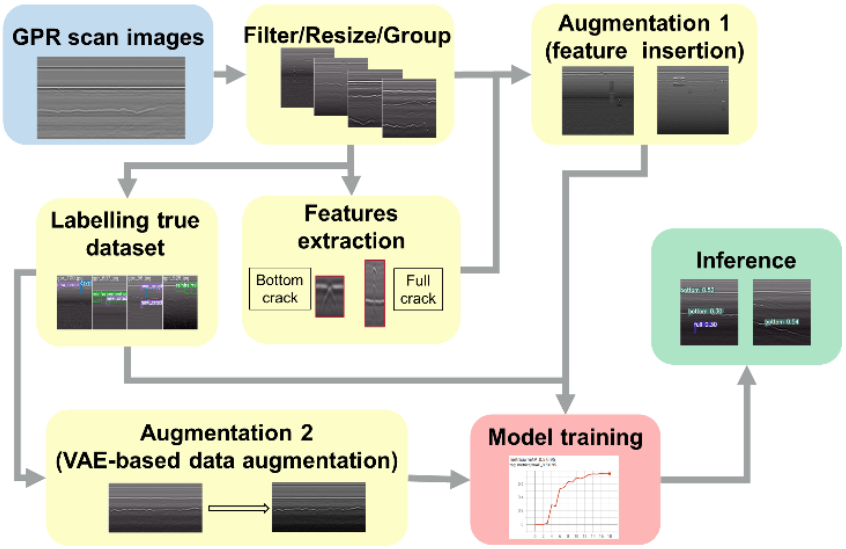

Figure 24 Data pipeline, model training and inference

In the dataset segmentation process, the collected data is categorized into two distinct groups: images featuring target features (termed "featured images") and images devoid of such features (referred to as "unfeatured images"). The featured images, crucial for model training, are manually labeled in compliance with the format requisite for YOLOR training. Meanwhile, the abundant unfeatured images are harnessed as background images, facilitating the creation of synthetic data by embedding extracted target feature patches.

As outlined in Figure 24, the data acquisition module (in blue) encompasses GPR image acquisition from scanned road sections. The dataset formation modules (in yellow) elucidate the incorporation of the two augmentation methods to acquire synthetic data. The model training and testing module (in pink) represents YOLOR model training and validation, and the module in green signifies the practical application of the trained model for inference.

4.3.1. Data augmentation with feature insertion

Within the context of object detection, there's a way to create artificial images with objects and labels, and it's called "feature insertion." This technique as depicted in Figure 25 allows us to generate images that look real but have specific desired objects.

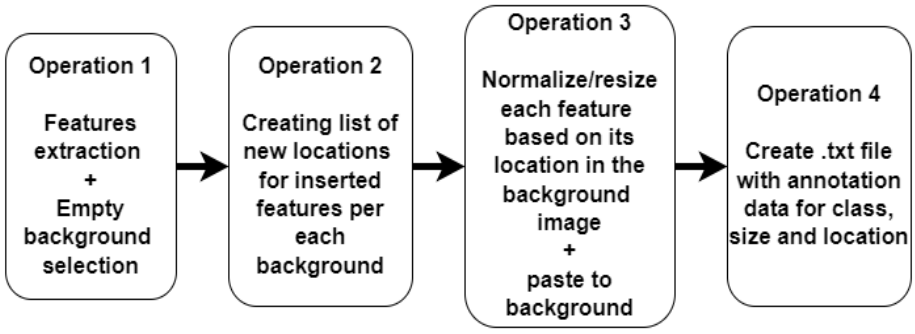

Figure 25 The process of generating synthetic data by feature insertion.

Here's how it works: The process starts with images that have nothing in them, just empty backgrounds as shown in Figure 26. These blank images are where the code put the objects needed to be detected.

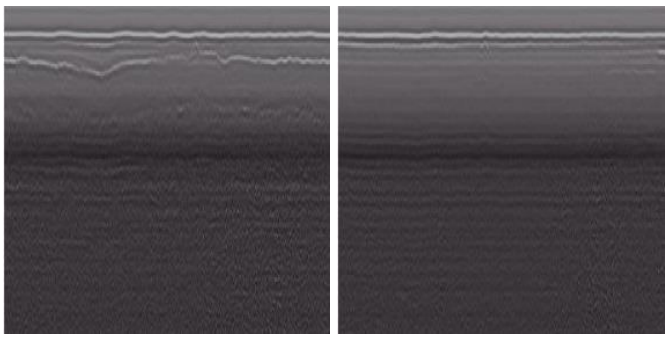

Figure 26 Empty background with no features for synthetic data creation

Next, the images of the inserted objects. These object images are like puzzle pieces, and carefully placed onto blank backgrounds. It's important to position them correctly, so they look like they're part of the scene and don't overlap.

To make these created images appear realistic, adjustments are made to the pixels. This can involve changing their size, stretching them, adjusting the colors, and blending them with the background. (Figure 27). This step ensures that the added objects fit naturally into the picture.

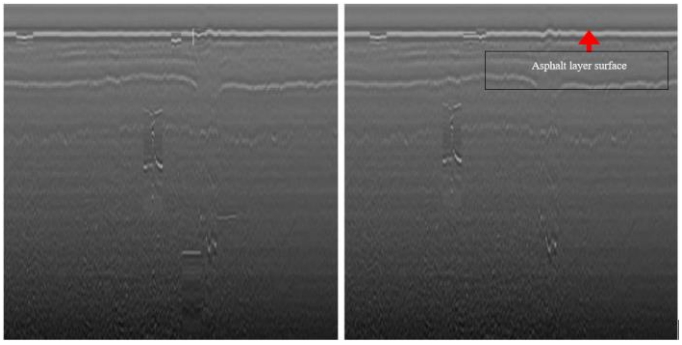

Figure 27 Example synthetic images generated by the algorithm

The neat part is that knowing where these objects are placed and what they represent allows for the automatic generation of labels. This eliminates the need for the time-consuming manual labeling of each image.

While this feature insertion method is handy, it has its limitations. Sometimes, the adjustments made can cause small imperfections around the edges of the added objects. Additionally, the artificial images created may not show a wide variety of the objects being detected. To address these limitations and make synthetic images appear more natural, another method called Variational Auto-Encoders (VAE) is explored, which will be discussed in the following section.

4.3.2. Data augmentation with generative models

Another approach to augment the dataset involves the use of generative models, specifically Generative Adversarial Networks (GANs) and Variational Autoencoders (VAE) (Goodfellow et al. (2014); Kingma and Welling (2013)). However, given the limited availability of featured

images for training a generative model, a modified VAE with specific design considerations was adopted. This approach enables the leverage of low-level feature information to generate new images. The architectural layout of the employed VAE is depicted in Figure 28.

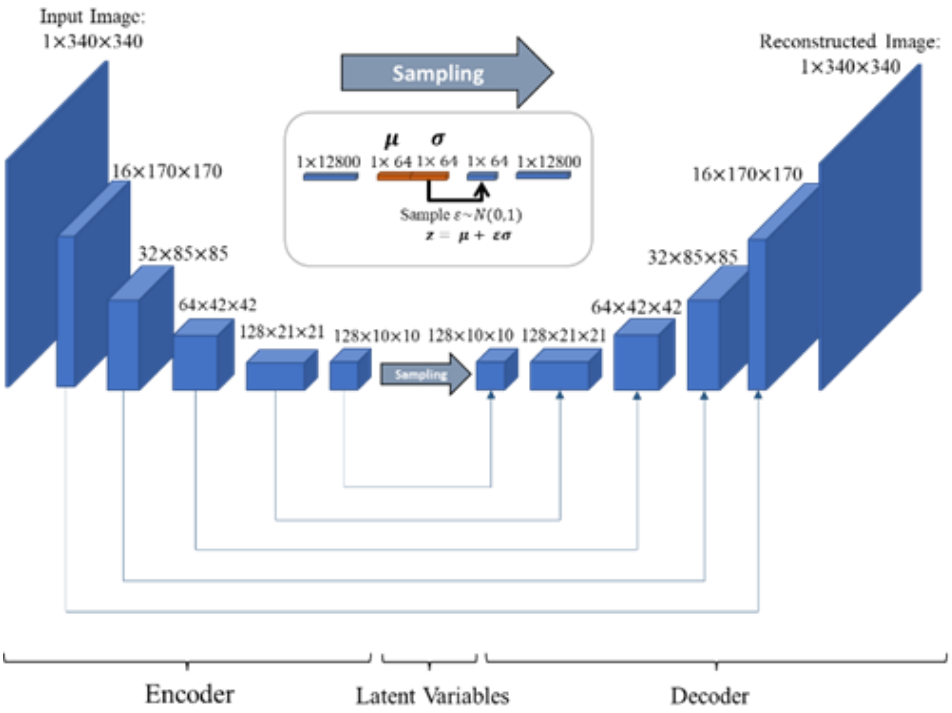

Figure 28 Variational autoencoder with shortcut connections

It's worth noting that while these VAE-generated images may lack diversity in terms of features, experiments have demonstrated that their inclusion in the dataset leads to improved model performance.

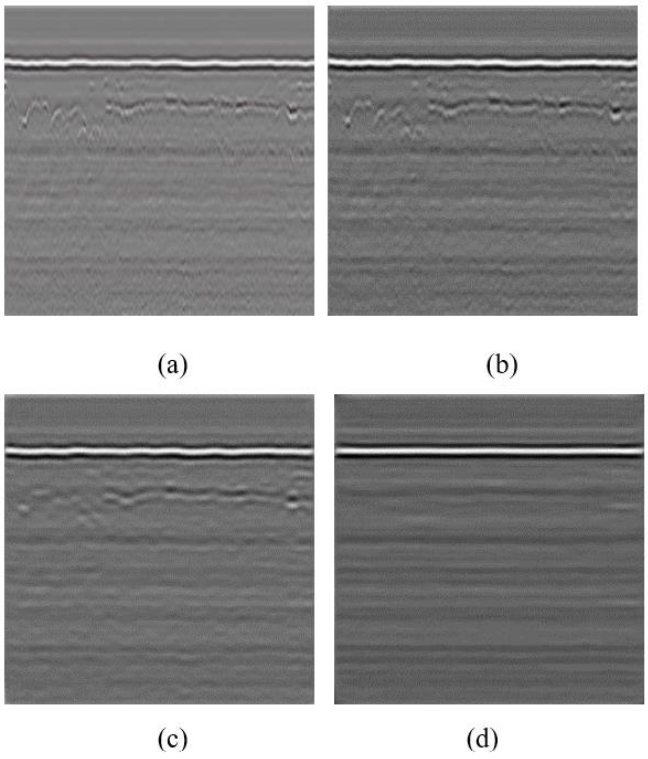

Figure 29 Comparison of (a) original image, (b) generated image with shortcut connections 1-3, and (c) generated image with shortcut connections 2-3, and (d) generated image out shortcut connection 3

Through the combination of both augmentation methods, a dataset comprising 9,174 GPR images has been amassed. This dataset has been partitioned into subsets for training, validation, and testing, as outlined in Table 11.

Table 11 Data Partition for Model Training, Validation, and Testing

Dataset	**# of images**	**Comment**
Train	7,674	All synthetic images
Validation	1,000	100 real featured images and 900 synthetic images
Test	500	All real images (400 featured images + 100 background images)
Total	9,174	The entire dataset includes a total of 23,272 target features

It is crucial to highlight that the training dataset exclusively consists of synthetic images, whereas the validation dataset incorporates a mixture of synthetic and real images. On the other hand, the

test dataset comprises solely real images, representing a comprehensive evaluation of the model's performance on real-world data.

4.4. YOLOR MODEL EXPERIMENT

For the object detection task, the YOLOR-P6 model was chosen. To enable the model to learn from existing knowledge, transfer learning was applied by initializing it with pretrained weights from the COCO dataset, which is widely used for object detection. Model training was conducted on a workstation equipped with an Intel(R) Xeon(R) CPU @ 2.30GHz, 13 GB of RAM, and an NVIDIA Tesla K80 GPU.

During training, the standard YOLOR loss function was utilized. Nevertheless, a modification was implemented to the classification head of the model to tailor it for the specific task of detecting two classes of cracks. To facilitate effective model training, the Adam optimizer was employed with a batch size of 8, and the initial learning rate was set at 0.001.

In object detection, a commonly used metric to assess performance is the Average Precision (AP) at Intersection over Union (IOU) = 0.5. AP measures how well the model performs by considering both precision and recall. Precision tells us the proportion of true positive detections among all the positive predictions, while recall tells us the proportion of true positive detections among all the actual positive instances. The formulas for precision and recall are shown in Equations (4-1) and (4-2), where TP represents true positives, FP is false positives, and FN stands for false negatives.

$$\text{Precision (specificity)} = TP / (FP + TP) \tag{4-1}$$

$$\text{Recall (sensitivity)} = TP / (FN + TP) \tag{4-2}$$

The training progress is visualized in Figure 30, demonstrating that the training process converged with a validation AP of 0.896.

To thoroughly assess the model's performance, the test dataset comprising only original featured images was utilized. The precision-recall curve for the test data is depicted in Figure 31. Model exhibited a similar level of performance on the test data, achieving APs@0.5 of 0.769 for all cracks, 0.803 for bottom cracks, and 0.735 for full cracks.

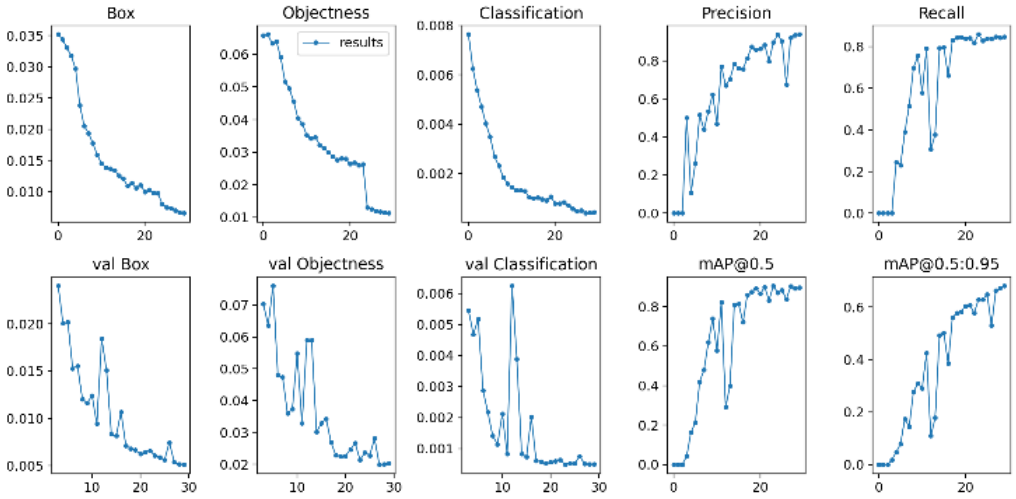

Figure 30 Training progress of the YOLOR model.

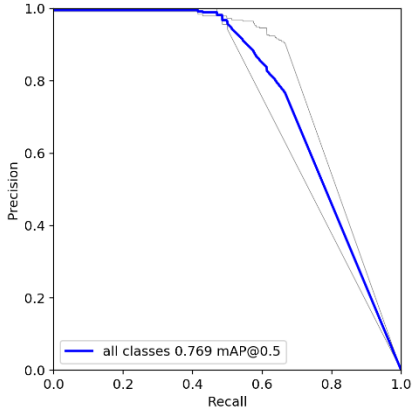

Figure 31 Precision-Recall curve.

This comprehensive evaluation demonstrates the effectiveness of YOLOR-based approach in accurately detecting subsurface cracks in pavement, with strong performance on both the validation and test datasets.

4.5. RESULTS AND CONCLUSION

Deep learning techniques, specifically the utilization of the YOLOR real-time object detection algorithm, were explored to automate the inspection of subsurface conditions in pavement. The primary goal of this endeavor is to enable timely detection of structural issues, particularly bottom-initiated cracks, to facilitate cost-effective repair and rehabilitation efforts.

A significant challenge faced throughout this research was the limited availability of high-quality target features needed for training the deep learning model. To tackle this issue, a meticulous preprocessing approach was employed on the collected GPR scan data. This involved filtering out sections that exhibited potential target features. Subsequently, these filtered scans underwent visual inspection to confirm the presence of the desired features, followed by manual annotation.

To address the scarcity of target features, two distinct data augmentation methods were implemented: feature insertion and feature generation. The feature insertion method facilitated the rapid expansion of the dataset without the need for labor-intensive manual labeling. It's important to note that the synthetic images generated by this method lacked diversity. In contrast, the feature generation method utilized a Variational Autoencoder (VAE) with shortcut connections to create images closely resembling the originals. Combining augmented data from both methods proved highly effective in improving the overall performance of the model.

Our trained model achieved a notable test Average Precision (AP) score of 0.769 for detecting all crack features within GPR scan images, even when trained exclusively on synthetic data. This achievement underscores the practicality and feasibility of utilizing synthetic data to train robust deep learning models for the detection of subsurface cracks.

Nevertheless, it's important to acknowledge the inherent limitations of both data augmentation methods. Further exploration into advanced generative models, such as conditional Generative Adversarial Networks (cGANs) and StyleGANs, holds the potential to generate more realistic and diverse featured images, thereby further enhancing model performance.

Looking to the future, there is potential to broaden the scope of this study by incorporating various underground characteristics, leading to a more comprehensive evaluation of pavement conditions. Furthermore, integrating the deep learning model with numerical models and data from other field tests, such as the falling weight deflectometer (FWD), can offer a more holistic assessment of pavement conditions. This integration would yield valuable insights that could assist in making informed decisions regarding maintenance and rehabilitation strategies, ultimately enhancing the accuracy and reliability of pavement condition assessments.

CHAPTER 5

SUBSURFACE DISTRESS PREDICTION FIELD VALIDATION

Interpreting GPR data can be challenging due to its complexity and the diversity of potential defects in pavements. Recent advancements in deep learning offer a promising solution by improving defect detection accuracy and reducing analysis time. Custom deep learning models tailored for GPR data can automate the extraction of relevant features and accurately identify subsurface cracks, such as "bottom-up" fatigue cracks.

In a prior study (Diamanti et al., 2010), researchers investigated vertical crack responses in various pavement conditions using GPR. They demonstrated GPR's capability to detect cracks, particularly in asphalt over granular materials.

The timely detection and remediation of pavement cracks are critical for preventing structural failures. Applying deep learning to GPR image analysis has shown promise in identifying concealed distresses within pavement layers.

However, two main challenges hinder effective GPR use for pavement assessment. Firstly, complex data pre-processing is required to extract relevant distress features. Secondly, human intervention is needed to handle the complex data background and foreground. Various data processing approaches, including Support Vector Machine (SVM) and S-Transform, have been

used to detect roadway disturbances in GPR data. These methods partially replace human inspections but still require some level of human intervention.

Developing an automated detection method that can consistently identify cracks under various real-world conditions is crucial for improving accuracy and efficiency in pavement assessment (Diamanti et al., 2010; Solla et al., 2014; Szymczyk et al., 2015; Xu et al., 2010; Zhou et al., 2013; Xue et al., 2013; Tosti and Benedetto, 2012).

5.1. GPR-AI PAVEMENT DISTRESS DETECTION

Advancements in non-destructive testing methods like GPR, FWD, and laser scanning have generated extensive pavement imagery and data, offering valuable insights into pavement conditions. Object detection-deep learning models have become indispensable for enhancing the analysis of this data. These models efficiently predict and identify subsurface distresses in pavements, providing accurate monitoring and issue localization. This aids governmental agencies and decision-makers in making informed choices about maintenance, repair, and rehabilitation, enabling the development of cost-effective pavement management strategies.

Deep learning has made significant strides across various domains, including pattern recognition, 3D objects retrieval, object location, and regressive computation. In structural and civil engineering, deep learning methods have found practical applications in detecting roadway disruptions. Cha et al. (2018) utilized Convolutional Neural Networks (ConvNet) for precise pavement crack detection under real conditions.

Similarly, Sha et al. (2016) introduced a ConvNet-based approach for detecting various types of road distress, while Tong et al. (2017, 2018) developed deep learning models for identifying,

locating, and reconstructing road disturbances in three dimensions. However, some studies reported unsatisfactory recognition accuracy, highlighting deep learning's limitations. Beckmann et al. (2019) developed an advanced deep learning technique combined with a structural surface fitting algorithm to automate volumetric damage quantification using a depth camera. The model demonstrated an average accuracy of 90.79% and a mean accuracy error of 9.45%. Deep learning's appeal lies in its stability, enabling recognition across varying features and backgrounds, and its automation, allowing autonomous learning of features related to object recognition.

This chapter delves into the research conducted to validate comprehensive approach for automating the acquisition of pavement distress data, achieved by integrating GPR with deep learning models. Building upon the foundation laid in the preceding chapter, which focused on identifying subsurface cracks within pavement layers using GPR images, methodology proposed within this research takes a proactive stance in detecting these defects even before they manifest on the pavement surface. The central emphasis of this research revolves around detecting and analyzing two primary categories of pavement distress: fatigue cracking and reflective cracking, leveraging the capabilities of GPR. Fatigue cracking is recognized by interconnected cracks that initiate at the base of the HMA layer, often resembling a network of transverse and longitudinal lines or polygons on the pavement's surface, eventually progressing to the topmost layer. Conversely, reflective cracking is observed in asphalt-surfaced pavements situated over a PCC base or an existing asphalt pavement. These cracks typically align with the cracks or joints in the underlying concrete or existing asphalt pavement. Once reflective cracking becomes visible, it tends to reoccur or extend further, particularly if the underlying base experiences ongoing movement or deterioration. This alignment serves as a clear indicator of the influence of the

underlying structure on surface cracks. Leveraging GPR's non-destructive capabilities, the effective monitoring of distress evolution, from their inception below the surface to gradual propagation towards the pavement's exterior, is achievable. The advantage of this comprehensive approach is its capability to identify distresses during their early stages, often before they become visible on the pavement surface. This early detection empowers transportation agencies to conduct more thorough assessments of pavement conditions and promptly implement maintenance and rehabilitation strategies.

5.2. IMAGE ENHANCEMENT TECHNIQUES

In chapter 4, this research was initiated by examining how GPR is employed to investigate pavement distress. This involved providing a detailed understanding of how images are obtained using GPR, thus offering valuable insights into the process.

Following that, various improvements were made to the GPR images. These enhancements were implemented with the goal of making it easier to detect pavement cracks, thereby enhancing the accuracy of crack detection methods.

Towards the end of this chapter, more insight was gained into the YOLOR model, which had been specifically customized and implemented for the purpose of pavement crack detection using GPR images. A detailed overview was provided of how this model was designed and developed, emphasizing its relevance and effectiveness within the context of GPR images.

To evaluate the GPR-YOLOR model, the criteria used for evaluation were also discussed. This enabled an assessment of both its accuracy and overall effectiveness in the context of this research.

5.2.1. Images Acquisition

High-resolution GPR images of pavement cracks were collected. The scanning was focused on the left wheel path, as indicated in Figure 32. This research considered all the cracks within this scanning area.

Figure 32 GPR scan line

Simultaneously, a dash camera with a resolution of 1920 x 1080 pixels, capturing video at 30 frames per second, recorded surface images. These images provided visual data of the asphalt surface while the GPR scan was conducted. The study concentrated on evaluating two specific road sections in Athens, GA, USA: Baxter Street (0.4 miles) and South Lumpkin Street (0.8 miles), with a combined length of 1.2 miles, as depicted in Figure 33.

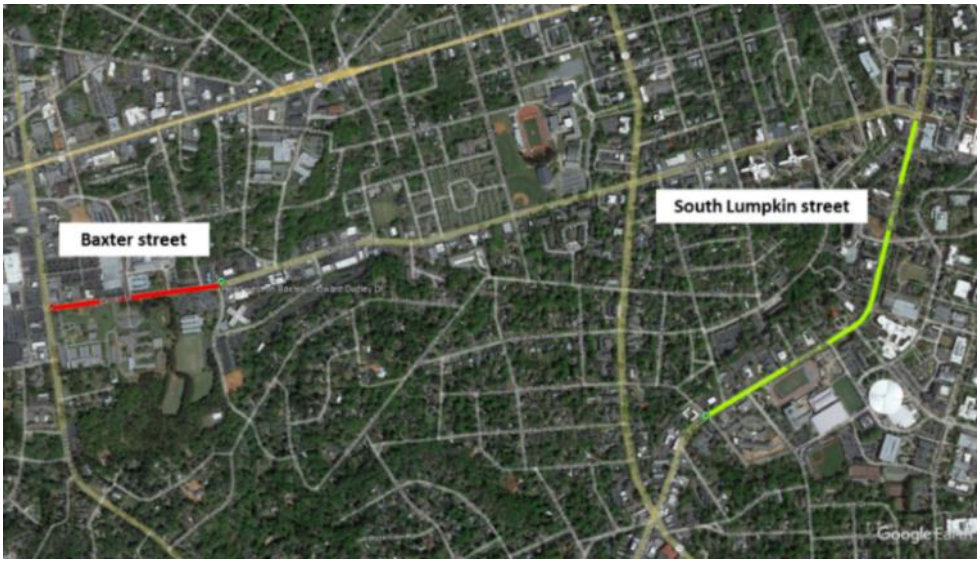

Figure 33 Test sections

To enhance the accuracy of pavement crack detection and ensure proper alignment with GPR images, surface images were acquired using a front shield dash camera. These surface images underwent preprocessing and optimization procedures to enable a thorough examination of pavement crack conditions and the precise validation of the GPR-YOLOR model's predictions regarding subsurface cracks. In the pursuit of creating a dependable autonomous model for detecting pavement distress, the availability of a high-quality GPR image database is of utmost importance. It's worth noting that the quality of GPR images can vary depending on the assessed pavement structure. Therefore, researchers generated GPR images under various conditions using a synthetic image creation method outlined in a previous study by Abdelmawla et al. in 2023.

5.2.2. GPR image enhancement

For this research, high-resolution GPR images of pavement cracks were obtained using an air coupled GPR antenna with a 2 GHz frequency. Unlike ground-coupled antennas, this choice aimed to improve the quality of GPR images, enhancing the deep learning model's ability to detect

subsurface pavement distress accurately. Additionally, a 20 ns time window was applied during data collection to capture detailed information within the pavement layers, particularly the asphalt and graded aggregate base (GAB). This detailed data allowed for a precise assessment of the pavement structure and the detection of potential distresses.

Identifying regions of interest within GPR images is vital in various research fields, including geology, civil engineering, and environmental science. To enhance the clarity, contrast, and noise reduction of these images, several enhancement techniques were applied. These techniques include Gaussian filtering, Contrast Limited Adaptive Histogram Equalization (CLAHE) (Zuiderveld, 1994), and Wiener filtering.

Here is a step-by-step description of the enhancement process:

1. A Gaussian filter with a 7x7 kernel size and a standard deviation of 0 was applied to the input image. This step aimed to reduce high-frequency noise in the image, improving the identification of regions of interest.
2. The smoothed image was converted to grayscale for further processing.
3. Contrast Limited Adaptive Histogram Equalization (CLAHE) was employed on the grayscale image. CLAHE enhances image contrast while mitigating noise amplification. It divides the image into tiles, performs histogram equalization on each tile, and then integrates them using bilinear interpolation. This process enhances contrast, aiding in the differentiation of different regions within the GPR image.

Figure 34 illustrates the division of the input image into tiles and demonstrates the subdivision of the image into four tiles as an example. This CLAHE technique effectively enhances the contrast of the GPR image, enabling better discernment between different regions.

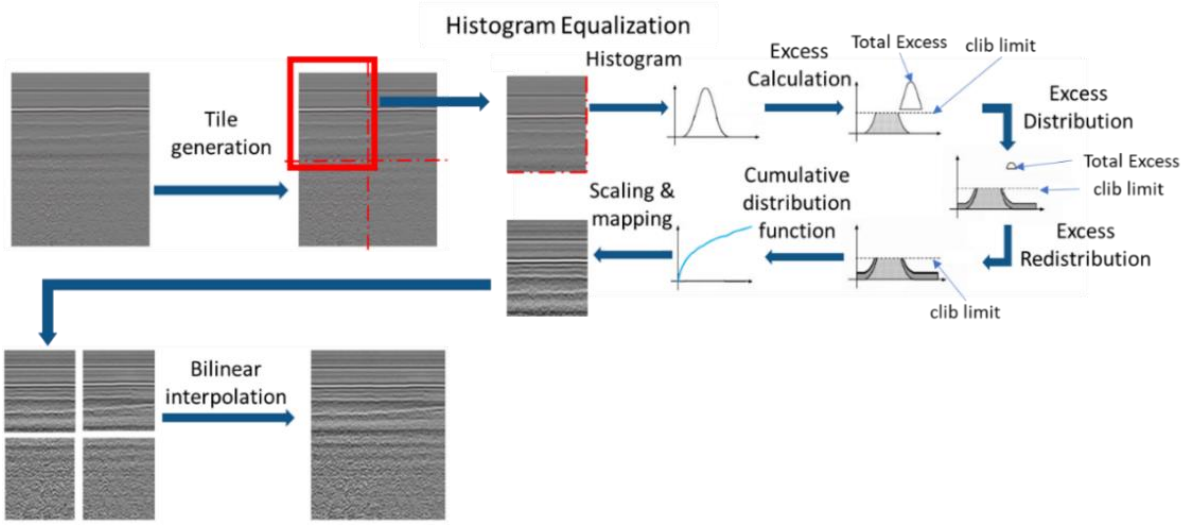

Figure 34 CLAHE Algorithm

4. Finally, a Wiener filter was used to further reduce noise and improve image quality. The Wiener filter operates in the frequency domain and estimates and subtracts noise from the original image, assuming that noise is uncorrelated with the signal. It effectively reduced remaining noise, resulting in an enhanced image with improved clarity and quality.

The Wiener filter is mathematically described by equation (5-1):

$$H(u,v) = \frac{1}{G(u,v)} \frac{|G(u,v)|^2}{|G(u,v)|^2 + K} \quad (5\text{-}1)$$

In this equation, H(u,v) represents the transfer function of the Wiener filter, G(u,v) corresponds to the Fourier transform of the input image in the frequency domain, and K is the Wiener filter parameter determining the trade-off between noise reduction and image sharpness.

By applying the Wiener filter, this research achieved noise reduction, leading to enhanced GPR images suitable for accurate region detection.

The combination of these image processing techniques, including the guided filter, Gaussian filter, and CLAHE, effectively improved the quality of GPR images for region detection. These techniques reduced noise while preserving critical features like edges, resulting in enhanced images suitable for various applications. Customizing the parameters of each technique allowed for tailored image enhancement based on specific research requirements. Figure 35 demonstrates the successful application of these techniques in enhancing GPR images.

The use of these enhancement techniques, alongside the choice of an air coupled GPR antenna and a defined time window, collectively contributed to improved image quality and enhanced accuracy in detecting subsurface pavement distress.

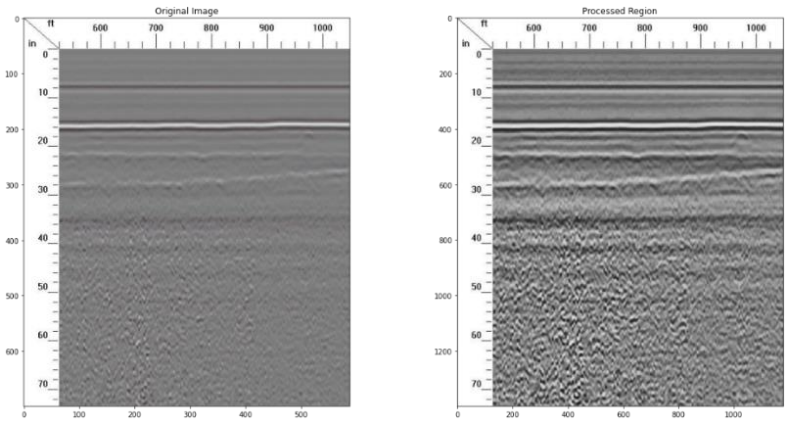

(a) (b)

Figure 35 GPR image enhancement example (a) before enhancement (b) after enhancement

5.2.3. Surface Image Processing

In the context of this research, surface images captured by commercial dashcams are employed to validate the predictions made by the GPR-YOLOR model regarding subsurface pavement

cracking. To ensure precise validation, these collected images are characterized by their coordinates, including latitude and longitude. This meticulous tagging allows for accurate alignment between identified surface cracks and the predicted locations of subsurface cracks. Proper alignment is crucial to enhance the usability of the collected images and to extract valuable information. It becomes especially important when misalignments could potentially hinder the interpretation of the image content.

A critical step in the image preprocessing pipeline is the application of perspective transformation. This transformation corrects inherent perspective distortions present in the captured images. The result is a top-down representation of the observed scene, as depicted in Figure 36. This corrected perspective enhances the detection of features and the interpretation of patterns within the images.

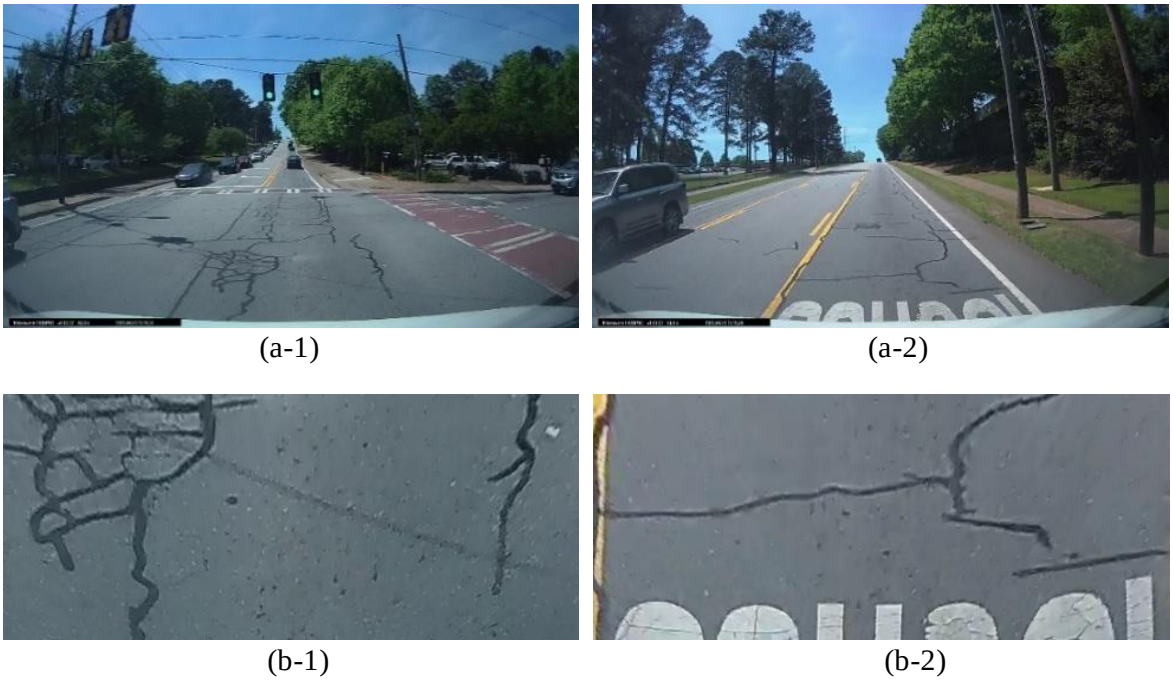

(a-1) (a-2)

(b-1) (b-2)

Figure 36 Surface images captured by dashcam in 2023

The transformation process, as shown in Figure 36, involves two sets of images: (a-1) and (a-2) representing the original images captured by the dashcam, and (b-1) and (b-2) denoting the selected region of interest within the scanned lane. Through this transformation, the images are adjusted to focus on specific areas of interest, allowing for more concentrated analysis and interpretation of relevant image content. This systematic and automated approach streamlines the correction of perspective distortion, making it feasible to conduct further analysis or processing of the transformed images for various research applications.

5.3. GPR-YOLOR MODEL

In Chapter 4, a pretrained YOLOR model was employed for the purpose of subsurface crack detection within pavement using GPR images. In response to the challenge of limited target data, two data augmentation methods were employed, namely feature insertion and generation. Feature insertion involved the creation of synthetic images through the insertion of subsurface cracks into object-free background images, and this process was accompanied by automatic label generation. On the other hand, data augmentation with generative models utilized a Variational Auto-Encoder (VAE) architecture, which was responsible for generating realistic featured images while preserving low-level target feature information.

In order to optimize the GPR-YOLOR model for the efficient and precise detection of subsurface cracks, a series of modifications were introduced to the configuration of the YOLOR model. These adjustments were tailored to meet the specific requirements of single-class detection within GPR images, ultimately resulting in enhancements in terms of efficiency, accuracy, and overall reliability.

5.3.1. Model Configuration

Incorporating changes to the model architecture, the number of filters utilized in the convolutional layers was adjusted, as elaborated in Table 12. This modification aimed to facilitate specialized feature representation that aligns with the characteristics of the target class found in GPR images. By simplifying the model in this manner, computational resources were utilized more efficiently, resulting in expedited inference and training processes.

Table 12 Changes over Modified code

Layer	YOLOR Filters	GPR-YOLOR Filters	YOLOR Classes	GPR-YOLOR Classes	YOLOR IOU Threshold	GPR-YOLOR IOU Threshold
203	256	256	80	1	0.213	0.5
204	384	384	80	1	0.213	0.5
205	512	512	80	1	0.213	0.5
206	640	640	80	1	0.213	0.5
207	255	18	-	-	-	-
208	255	18	-	-	-	-
209	255	18	-	-	-	-
210	255	18	-	-	-	-

Furthermore, an alteration was made to the Intersection Over Union (IOU) threshold applied in non-maximum suppression. This change involved increasing the threshold value, thereby establishing a more stringent criterion for accepting detection proposals. The primary objective of this adjustment was to mitigate the occurrence of multiple overlapping detections, thereby augmenting the model's precision. This refinement proved particularly beneficial in single-class detection scenarios, where GPR images typically contain fewer instances of closely located targets.

Introducing Region of Interest (ROI) functionality into the detection module enabled selective processing and analysis of objects within predefined areas of interest. This functionality primarily focused on the top asphalt layer, where subsurface cracks are most prevalent. As a result, the accuracy of the model was enhanced, and the occurrence of false detections reduced, even in scenarios characterized by complexity, multiple objects, or cluttered backgrounds as shown in Figure 37.

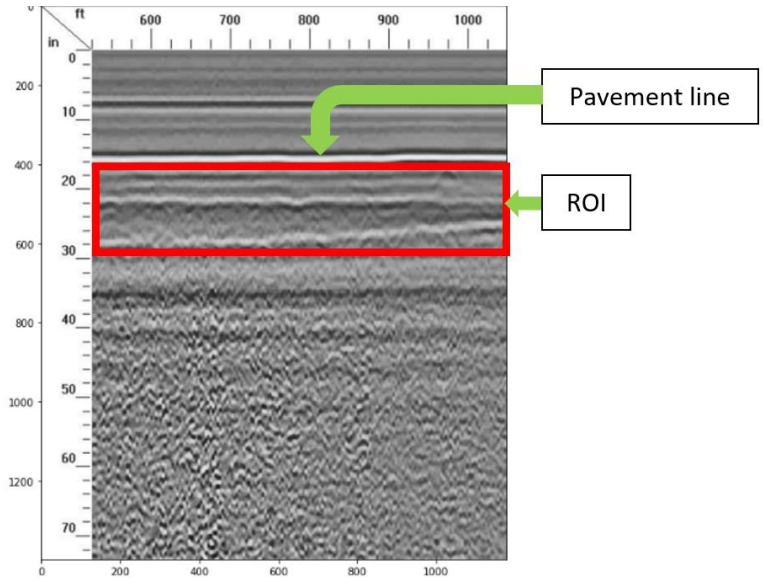

Figure 37 ROI in GPR images

The incorporation of ROI functionality within the GPR-YOLOR model contributed to resource optimization, particularly in resource-constrained environments or real-time applications. This enhancement led to improved processing times and overall operational efficiency. Additionally, the ROI feature offered flexibility and adaptability, empowering users to define and modify the ROI according to specific requirements and contextual scenarios. This adaptability widened the model's applicability, enhancing its versatility across a broader spectrum of use cases.

5.3.2. Evaluation Criteria

Evaluating GPR-YOLOR model's effectiveness in detecting subsurface cracks relies on three fundamental metrics: specificity, sensitivity, and F1 score, as denoted by equations (4-1), (4-2), and (5-2), respectively. Sensitivity gauges the model's capability to correctly identify positive instances, specifically the presence of subsurface cracks. Conversely, specificity assesses the model's precision in correctly recognizing negative instances, which correspond to areas devoid of subsurface cracks (see Figure 38). The F1 score offers a comprehensive evaluation of the model's overall performance by harmonizing both sensitivity and specificity.

$$\text{F1 Score} = \frac{2*\text{Specificity}*\text{Sensitivity}}{\text{Specificity}+\text{Sensitivity}} \tag{5-2}$$

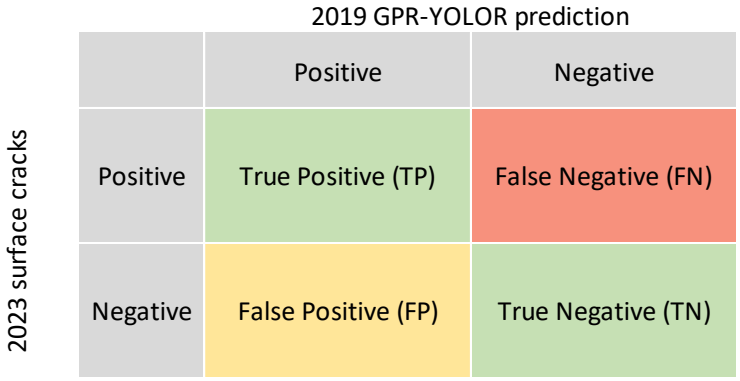

Figure 38 Confusion matrix

The evaluation procedure involves comparing the GPR-YOLOR model's predictions of subsurface cracks in the 2019 GPR scan images with the surface cracks that manifested on the pavement surface in the 2023 dashcam images. The association between subsurface and surface cracks is established based on their corresponding latitude and longitude coordinates. The meticulous process of precisely localizing each subsurface crack in the 2019 GPR images and retrieving the

corresponding coordinates for the 2023 surface cracks from the dashcam images is carried out. The alignment of these cracks is achieved through a nearest latitude and longitude approach.

The matching process comprises four key steps. Initially, Optical Character Recognition (OCR) is employed to extract the scan numbers from the top section of each GPR image (Figure 39). Subsequently, data refinement and processing techniques are applied to enhance the accuracy and utility of the extracted text.

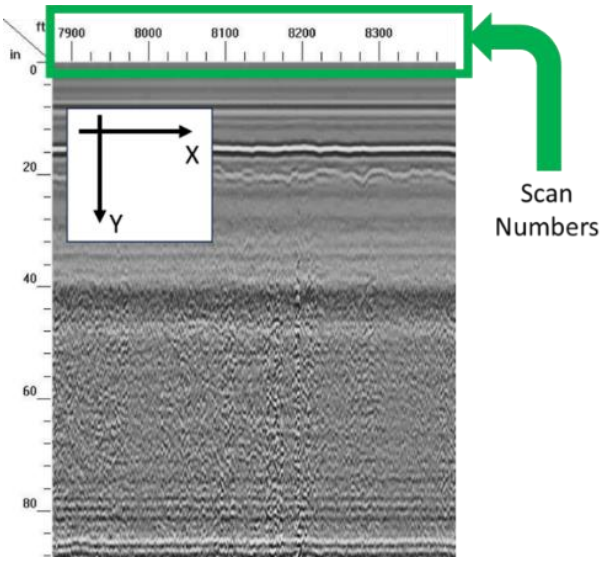

Figure 39 GPR image coordinates configuration

The second step involves determining the precise horizontal location (x-coordinate) of each scan number within the GPR image. This step ensures that each x-coordinate corresponds to a matching scan number from the top section of the image.

In the third step, each scan number is linked with its respective latitude and longitude coordinate from the collected GPR data. This is achieved by utilizing the text outputs from the GPR-YOLOR model in YOLO format, which represents the features detected within each specific GPR image

as (c x y w h) values – where they represent (class x-location y-location width height) respectively, for each detected object normalized to image dimensions. The association between the extracted features and their corresponding scan numbers, based on their x-coordinate location within the image, enables the precise attribution of latitude and longitude coordinates to each detected object.

The fourth and final step involves employing the GPS-tagged surface images from the dashcam, which provide accurate latitude and longitude information for each image. This facilitates a precise matching process between the surface images and the detected subsurface cracks obtained from the GPR-YOLOR model, based on their respective coordinates.

By combining the GPS-tagged surface images with the GPR-YOLOR model's output, a robust correspondence between the predicted subsurface cracks in 2019 and their corresponding surface cracks in 2023 is established. This comprehensive approach not only validates the model's accurate prediction of subsurface cracks but also enables the assessment of its performance over time as surface cracks emerge and evolve.

5.4. GPR-YOLOR IMPLEMENTATION

A case study encompassed two distinct phases of data collection and analysis conducted in 2019 and 2023. In 2019, GPR-based detection was employed, utilizing acquired images to predict subsurface cracks within the asphalt pavement layer. Subsequently, in 2023, surface images were captured to validate the accuracy and reliability of these predictions. The trained model was applied to the 2019 GPR data to predict subsurface images that were not visible on the surface at that time. This was due to the addition of a new pavement layer to the road, resulting in a clean

surface devoid of cracks. However, by 2023, surface cracks became apparent (see Figure 40) due to the propagation of the underlying cracks.

In the subsequent sections, outcomes from the methodologies for GPR image acquisition and enhancement are presented. Additionally, the performance evaluation of the deep learning model in detecting pavement distress is provided.

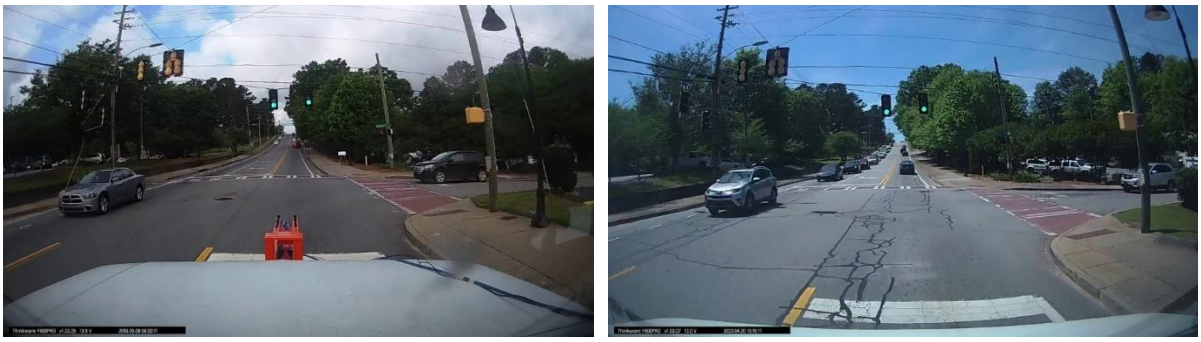

(a) (b)

Figure 40 Surface images captured by dashcam at the same location (a) 2019 survey, (b) 2023 survey.

Our evaluation focuses on assessing the model's accuracy and reliability in detecting subsurface cracks within the asphalt pavement layer. To accomplish this, a comparison is made between the model's performance in subsurface crack detection and its performance in detecting surface cracks at the same coordinates. This comparative analysis facilitates a comprehensive evaluation of the model's capabilities.

5.4.1. Crack detection in GPR images

The application of enhancement techniques to the GPR images significantly improved several critical aspects, including clarity, contrast, and noise reduction. These enhancements resulted in more precise identification of regions that are pertinent to the detection of subsurface pavement distress. The GPR-YOLOR model, based on Abdelmawla et al.'s (2023) prior research,

demonstrated an enhanced level of accuracy in subsurface crack detection. This improvement is evident in Figure 41, where a notable difference in the model's performance can be observed.

Figure 41 provides a comparison between two sets of images: (a-1) and (b-1) represent detection outcomes before the application of enhancement techniques, while (a-2) and (b-2) depict detection outcomes after the enhancement process.

This comparison distinctly highlights the model's superior performance in identifying a greater number of subsurface cracks after the enhancement procedures were implemented.

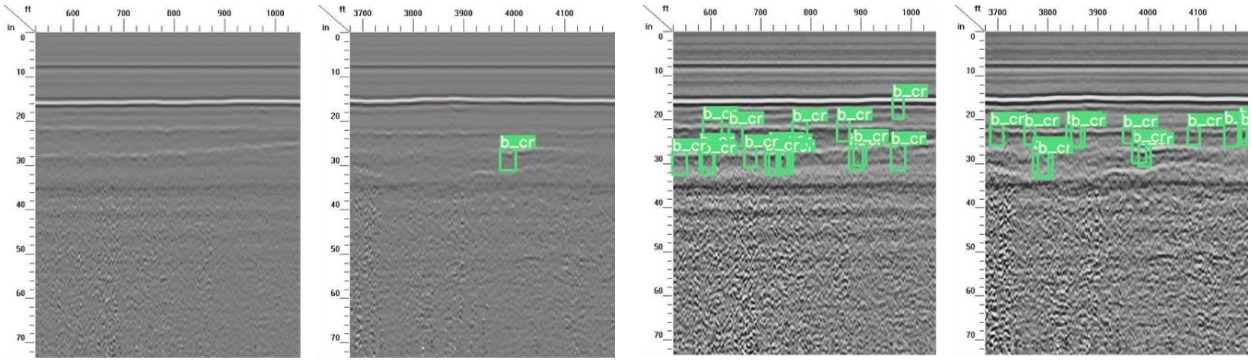

(a-1) (a-2) (b-1) (b-2)

Figure 41 (a) detection before enhancement, (b) detection after enhancement

5.4.2. Model field performance

This research study was centered around the task of detecting subsurface cracks using the GPR-YOLOR model, an extension of Abdelmawla et al.'s (2023) The refinement of GPR images played a pivotal role in significantly enhancing the model's accuracy in identifying subsurface cracks. Furthermore, processed surface images, featuring informative visualizations as shown in Figure 42, were employed to validate the presence of surface cracks. The integration of the image processing framework with the GPR-YOLOR model enabled a comprehensive comprehension of

pavement distress. This holistic approach supports targeted maintenance interventions, ensuring the long-term sustainability and durability of transportation infrastructures.

(a) (b)

Figure 42 Surface images with cracks detected, (a) original image, (b) processed image.

To assess the performance of the GPR-YOLOR model in detecting pavement subsurface cracks, various metrics were employed, as shown in Table 13. The model achieved a precision of 0.76, recall of 0.68, and an F1 score of 0.72. These metrics were computed by comparing the model's predictions to the corresponding surface cracks, which served as pseudo labels. Precision indicates the proportion of correctly identified cracks among all the model-detected cracks, while recall measures the proportion of correctly identified cracks among all the actual cracks present. The F1 score provides an overarching measure of the model's performance, considering both precision and recall.

Table 13 Model performance evaluation parameters

	Baxter	**Lumpkin**	**Average**
Sensitivity (recall)	68.75%	67.94%	68.35%
Specificity (precision)	72.67%	79.42%	76.05%
F1 score	0.71	0.73	0.72

Table 13 presents the model's performance evaluation parameters, including sensitivity (recall), specificity (precision), and the F1 score for the Baxter and Lumpkin Street test sections, along with their average values. Sensitivity (recall) exhibited values of 68.35%, indicating the model's capability to detect subsurface cracks. Specificity values were 76.05%, indicating precise identification of non-crack areas. The F1 score of 0.72 further corroborated the model's effectiveness in autonomously detecting subsurface cracks within pavement layers. These results underscore the GPR-YOLOR model's proficiency in the task of detecting pavement subsurface cracks.

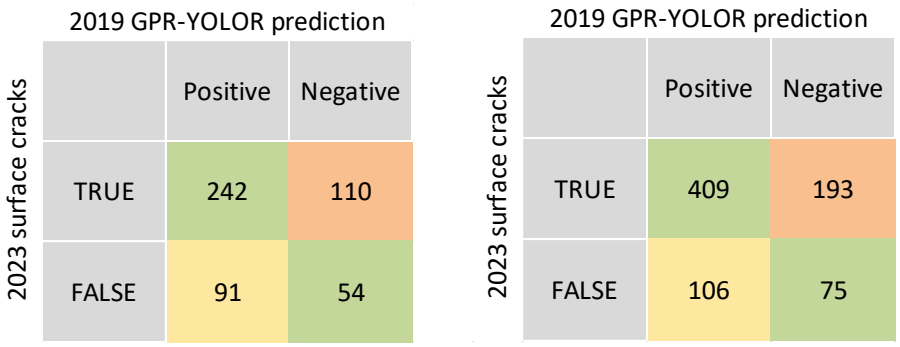

(a) (b)

Figure 43 Confusion matrix for GPR-YOLOR model (a) Baxter Street, (b) Lumpkin Street

The confusion matrices for the GPR-YOLOR model are displayed in Figure 43, depicting its accuracy on Baxter Street and South Lumpkin Street. These matrices offer a visual representation of the model's performance in distinguishing between true positives, true negatives, false positives, and false negatives, further confirming its capability in detecting pavement subsurface cracks.

5.5. VALIDATION SUMMARY

The integration of Ground-Penetrating Radar (GPR) scanning and advanced deep learning techniques in the proposed GPR-YOLOR model presents a highly promising and practical solution

for subsurface crack detection. It empowers decision-makers with essential subsurface information, streamlining pavement evaluation processes, and facilitating the implementation of effective maintenance and rehabilitation strategies. The potential impact of this approach on the infrastructure industry is profound, as it enables proactive and cost-effective maintenance practices, ultimately leading to the development of safer and more resilient road networks.

Furthermore, the model's practical applicability within maintenance workflows is bolstered by its real-time implementation and field validation. Subjecting the model to real-world conditions demonstrates its utility and reliability, establishing it as a valuable tool for pavement evaluation and maintenance planning. Looking ahead, future research should prioritize the expansion of datasets to enhance the model's performance, providing a more comprehensive understanding of pavement distress by incorporating multi-modal data sources. Additionally, the refinement of image enhancement techniques will be pivotal in further elevating detection accuracy. The exploration of transfer learning approaches will empower the model to effectively leverage pre-existing knowledge, optimizing its performance for specific scenarios and enhancing its versatility.

The GPR-YOLOR model introduces exciting possibilities in the field of subsurface crack detection. Its fusion of advanced deep learning and GPR scanning capabilities, coupled with its potential for real-time implementation and field validation, holds the promise of revolutionizing pavement evaluation and maintenance practices. As continued investments are made in research and development, models of this nature will undoubtedly make significant contributions to the establishment of safer and more resilient road networks, ensuring the long-term sustainability of critical infrastructure.

CHAPTER 6

CONCLUSIONS AND RECOMMENDATIONS

6.1. SUMMARY OF FINDINGS

A thorough investigation was undertaken to harness the potential of Ground-Penetrating Radar (GPR) technology in assessing the physical parameters of subgrade layers and detecting subsurface anomalies within pavement structures. The key findings of this study are succinctly outlined below, underscoring the substantial impact of this research in pushing the boundaries of pavement infrastructure evaluation.

Throughout this research endeavor, the utilization of GPR data in the assessment of subgrade layer physical parameters has been demonstrated. This innovative approach provides valuable insights into the subsurface conditions of road construction projects, enabling more informed decision-making processes. The GPR-Density model, derived through rigorous laboratory calibration and field validation, has exhibited promising accuracy in estimating dry density, particularly for fine-grained soil types. This achievement signifies a significant advancement in the realm of non-destructive testing methodologies, contributing to the enhancement of infrastructure quality and longevity.

Furthermore, the research introduced the GPR-YOLOR model, a novel deep learning framework tailored specifically for the detection of subsurface abnormalities, notably pavement cracks, using

GPR images. The GPR-YOLOR model, coupled with sophisticated image enhancement techniques, has showcased remarkable performance improvements in identifying subsurface distress, addressing a critical challenge in pavement assessment and maintenance. This innovation has the potential to revolutionize the efficiency and accuracy of infrastructure inspection, ensuring the early detection of structural issues and facilitating timely remediation.

6.2. CONTRIBUTIONS TO THE FIELD

This research has made several substantial contributions to the field of civil engineering and pavement infrastructure assessment:

A. Advancement in Subgrade Evaluation: The development and application of the GPR-Density model provides an innovative and non-invasive approach to assess subgrade layer physical parameters, particularly dry density. Leveraging the advantages of Ground-Penetrating Radar (GPR), this model enhances the accuracy and efficiency of construction quality control while facilitating informed decision-making in road construction projects. This novel method represents a significant step forward in the realm of non-destructive subgrade assessment.

B. Enhanced Pavement Assessment: The introduction of the GPR-YOLOR model, in conjunction with various image enhancement techniques, signifies a remarkable advancement in pavement assessment. This deep learning framework substantially improves the reliability and speed of subsurface distress detection, thereby contributing to more effective and responsive roadway maintenance strategies. It offers a practical solution to a critical challenge in pavement evaluation.

C. Real-world Implementation: This research successfully bridges the divide between theoretical advancements and practical application. Through extensive field tests and validation exercises, the models developed in this study have demonstrated their effectiveness in real-world scenarios. This real-world implementation aspect underscores the relevance and utility of the research outcomes in addressing practical infrastructure assessment and maintenance needs.

D. Potential for Future Research: By candidly acknowledging the limitations and challenges encountered during the course of this study, such as the imperative for expanded datasets and the ongoing refinement of image enhancement techniques, this research serves as a catalyst for future investigations in the domain of GPR-based infrastructure evaluation. The identified research gaps and areas requiring further exploration lay the foundation for continuous advancements in non-destructive testing methodologies and their application in infrastructure assessment.

6.3. LIMITATIONS AND FUTURE DIRECTIONS

While this research has achieved significant milestones in GPR-based infrastructure assessment, it is essential to acknowledge its limitations and outline potential avenues for future research:

A. Mechanical Properties: While the research successfully identifies essential physical properties of different subgrade layers, including dry density and water content, further investigations are warranted to assess the mechanical properties of various pavement layers. This includes factors like pavement strength, modulus, and resilience, which are critical for structural evaluations.

B. Integration with Other Technologies: Future research endeavors should explore the seamless integration of GPR data with other non-destructive testing technologies. This synergistic approach would provide a more comprehensive assessment of infrastructure health, combining GPR's subsurface insights with data from complementary technologies.

C. Limited Dataset: The research acknowledges the limitation of a relatively small and less diverse dataset for both subgrade assessment and subsurface distress detection, such as cracks or abnormalities. Future research should prioritize the acquisition of a larger and more diverse dataset, which would significantly enhance the accuracy and generalizability of the developed models.

D. Image Enhancement Techniques: Ongoing research efforts should focus on refining and expanding image enhancement techniques to address varying pavement conditions and GPR data quality issues. Further advancements in image enhancement can lead to more robust models capable of handling a broader range of real-world scenarios.

E. Network-Level Assessment: Extending the application of the GPR-Density and GPR-YOLOR models to network-level road assessment represents a valuable direction for research. Scaling up the models for broader infrastructure maintenance planning at the network level would enable more efficient and proactive maintenance strategies.

F. Remote Sensing Integration: The integration of remote sensing and satellite imagery analysis techniques with GPR reflection calculations offers an intriguing avenue for further research. Exploring how satellite imagery can complement GPR data for pavement

condition assessment can lead to innovative and cost-effective approaches for large-scale infrastructure monitoring and management.

In summary, while this research has made substantial strides in GPR-based infrastructure assessment, there exist promising opportunities for future research to address these limitations and expand the horizons of non-destructive testing methodologies in civil engineering and pavement maintenance. These directions pave the way for more comprehensive, efficient, and holistic approaches to infrastructure assessment and management.

REFERENCES

1. AASHTO. Guide for design of pavement structures, Washington, D.C. 1993.
2. Abdelmawla, A.M., Durham, S.A. and Kim, S., (2019), Estimation of Subgrade Soil Density Using Ground Penetrating Radar. 2019 ICSC Conference Proceedings, Seoul, July 2019, Article no. A.5.3.
3. Abdelmawla, A.M. and Kim, S., (2020), Application of Ground Penetrating Radar to Estimate Subgrade Soil Density. Infrastructures, 5(2), 12.
4. Abdelmawla, A., Ma, S., Yang, J. J., & Kim, S. S. (2023). Subsurface anomaly detection utilizing synthetic GPR images and deep learning model. GEOMECHANICS AND ENGINEERING, 33(2), 203-209.
5. Al-Nuaimy W., Y. Huang, M. Nakhkash, M. T. C. Fang, V. T. Nguyen, and A. Eriksen (2000), "Automatic detection of buried utilities and solid objects with GPR using neural networks and pattern recognition", Journal of Applied Geophysics, vol. 43, no. 2–4, pp. 157–165.
6. Al-Qadi, I. L., Leng, Z., Lahouar, S., & Baek, J., (2010), In-Place Hot-Mix Asphalt Density Estimation Using Ground-Penetrating Radar. Transportation Research Record, 2152(1). 19–27. https://doi.org/10.3141/2152-03.
7. Amaghani, D., Mamou, A., Maraveas, C., Roussis, P., Siorikis, V., Skentou, A., & Asteris, P. (2021). "Predicting the unconfined compressive strength of granite using only two non-destructive test indexes", Geomechanics and Engineering, 25(4), 317–330. https://doi.org/10.12989/gae.2021.25.4.317
8. Ana, Luisa, Aranha., Liedi, Légi, Bariani, Bernucci., Kamilla, Vasconcelos. (2023). Effects of Different Training Datasets on Machine Learning Models for Pavement Performance Prediction. Transportation Research Record, doi: 10.1177/03611981231155902

9. ASTM D2487-17, Standard Practice for Classification of Soils for Engineering Purposes (Unified Soil Classification System), ASTM International, West Conshohocken, PA, 2017, www.astm.org

10. Benedetto A. and S. Pensa (2007), "Indirect diagnosis of pavement structural damages using surface GPR reflection techniques", Journal of Applied Geophysics, vol. 62, no. 2, pp. 107–123.

11. Benedetto, A., & Pajewski, L., (2015), Civil engineering applications of ground penetrating radar. Switzerland: Springer.

12. Beutel, R., Reinhardt, H.W., Grosse, C.U., Glaubitt, A., Krause, M., Maierhofer, C., Algernon, D., Wiggenhauser, H., Schickert, M., (2008). Comparative performance tests and validation of NDT methods for concrete testing. Journal of Nondestructive Evaluation 27, 59–65.

13. Cancan, Yi., Jun, Liu., Hui, Guan. (2023). An Efficient Method of Pavement Distress Detection based on Improved YOLOv7. Measurement Science and Technology, doi: 10.1088/1361-6501/ace929

14. Charalambos, Kyriakou., Symeon, E., Christodoulou. (2022). A low-cost pavement rating system, based on machine learning, utilizing smartphones sensors. Proceedings of the Institution of Civil Engineers, doi: 10.1680/jsmic.21.00030

15. Chen S., H. Wang, F. Xu, and Y.-Q. Jin (2016), "Target classification using the deep convolutional networks for SAR images", IEEE Transactions on Geoscience and Remote Sensing, vol. 54, no. 8, pp. 4806–4817.

16. Chenxi, Chen., Yang, Song., Yizhuang, David, Wang., Xianbiao, Hu., Jenny, Liu. (2023). A machine learning-based approach to assess impacts of autonomous vehicles on pavement roughness, doi: 10.1098/rsta.2022.0176

17. Dérobert, X., Iaquinta, J., Klysz, G., Balayssac, J.P., (2008). Use of capacitive and GPR techniques for the non-destructive evaluation of cover concrete. NDT & E International 41, 44–52.

18. Dérobert, X., Berenger, B., (2010_. Non-destructive evaluation of reinforced concrete structures: Non-destructive testing methods. Woodhead Publishing Series in Civil and Structural Engineering No. 35, Germany. Vol. 2. Chapter 25. pp. 574–584.

19. Diamanti N., D. Redman and A. Giannopoulos (2010), "A study of GPR vertical crack responses in pavement using field data and numerical modelling", Proceedings of the XIII International Conference on Ground Penetrating Radar, Castello Carlo V, Lecce, Italy, June.

20. Ding J., B. Chen, H. Liu, and M. Huang (2016), "Convolutional neural network with data augmentation for SAR target recognition", IEEE Geoscience and Remote Sensing Letters, vol. 13, no. 3, pp. 364–368.

21. EN ISO 14688-2:2004/A1:2013 "Geotechnical investigation and testing – Identification and classification of soil – Part 2: Principles for a classification – Amednment 1". Comité Européen de Normalisation. Brussels, 2004.

22. EN ISO 14688-1:2002/A1:2013 "Geotechnical investigation and testing – Identification and classification of soil – Part 1: Identification and description – Amendment 1". Comité Européen de Normalisation. Brussels, 2013.

23. Evans, Robert D., (2010), Optimizing Ground Penetrating Radar (GPR) to assess pavements. Loughborough University. Thesis. https://hdl.handle.net/2134/20465.

24. Gamba P., and S. Lossani (2000), "Neural detection of pipe signatures in ground penetrating radar images", IEEE Transactions on Geoscience and Remote Sensing, vol. 38, no. 2, pp. 790–797.

25. GDOT Transportation Asset Management Plan FY 2019 – 2028, Georgia, USA. http://www.dot.ga.gov/IS/TAM accessed on 11/12/2020.

26. Girshick R., J. Donahue, T. Darrell, and J. Malik, (2014), "Rich feature hierarchies for accurate object detection and semantic segmentation", Proceedings of the 2014 IEEE Conference on Computer Vision and Pattern Recognition, Columbus, OH, USA, June.

27. Goodfellow I. J., J. Pouget-Abadie, M. Mirza, B. Xu, D. Warde-Farley, S. Ozair, A. Courville, Y. Bengio (2014), "Generative adversarial networks.", arXiv:1406.2661.

28. Hogentogler, C.A.;Terzaghi, K. "Interrelationship of load, road and subgrade", Public Roads: 37–64, 1929.

29. Karras T., S. Laine, and T. Aila (2018), “A Style-Based Generator Architecture for Generative Adversarial Networks.”, arXiv:1812.04948

30. Karras T., M. Aittala, J. Hellsten, S. Laine, J. Lehtinen, and T. Aila (2020), “Training Generative Adversarial Networks with Limited Data.”, arXiv:2006.06676

31. Karras T., M. Aittala, S. Laine, E. Härkönen, J. Hellsten, J. Lehtinen, and T. Aila (2021), “Alias-Free Generative Adversarial Networks.”, arXiv:2106.12423

32. Kingma D. P., M. Welling (2013), “Auto-encoding variational bayes.”, arXiv preprint arXiv:13126114.

33. Kong, S. M., Kim, D. M., Lee, D. Y., Jung, H. S., & Lee, Y. J. (2018). “Field and laboratory assessment of ground subsidence”, Geomechanics and Engineering, 16(3), 285–293. https://doi.org/10.12989/GAE.2018.16.3.285

34. Krizhevsky A., I. Sutskever, and G. E. Hinton (2012), “ImageNet classification with deep convolutional neural networks”, Proc. Advances in Neural Information Processing Systems, vol. 25, pp. 1090–1098.

35. Kwon, S. Y., Yoo, M., & Hong, S. (2020), “Earthquake risk assessment of underground railway station by fragility analysis based on numerical simulation”, Geomechanics and Engineering, 21(2), 143–152. doi.org/10.12989/gae.2020.21.2.143

36. Lee, K. H., Park, J. H., Park, J., Lee, I. M., & Lee, S. W. (2022), “Experimental verification for prediction method of anomaly ahead of tunnel face by using electrical resistivity tomography”, Geomechanics and Engineering, 20(6), 475–484. https://doi.org/10.12989/gae.2020.20.6.475

37. Li, J., Gu, J., Huang, Z., Wen, J. (2019), “Application Research of Improved YOLO V3 Algorithm in PCB Electronic Component Detection.”, Appl. Sci., 9, 3750.

38. Lihui, Bai., Jie, Zhang., Xuwen, Zhu., Md., Morshedul, Alam., Zhihui, Sun. (2023). A machine learning ensemble model for predicting pavement conditions using automatic laser crack measurement data. International Journal of Pavement Engineering, doi: 10.1080/10298436.2023.2188591

39. Maierhofer, C., (2010). Planning a non-destructive test programme for reinforced concrete structures. Woodhead Publishing Limited. Vol. 2. Chapter 1. pp. 3–13.

40. Mohammad, Z., Bashar., Cristina, Torres-Machi. (2022). Deep learning for estimating pavement roughness using synthetic aperture radar data. Automation in Construction, doi: 10.1016/j.autcon.2022.104504

41. Mirza M., S. Osindero (2014). "Conditional generative adversarial nets.", arXiv:1411.1784.

42. Nanning, Guo., Lingyun, You., Zhengwu, Long., Songtao, Lv., Aboelkasim, Diab, (2023), Computationally Affordable Unsupervised Machine Learning Algorithm to Identify the Level of Distress Severity in Pavement Functional Performance. doi: 10.1109/TITS.2023.3253845

43. National Academies of Sciences, Engineering, and Medicine., (2009), NDT Technology for Quality Assurance of HMA Pavement Construction. Washington, DC: The National Academies Press. https://doi.org/10.17226/14272.

44. Ning, Chen., Zijin, Xu., Zhu, Liu., Yihan, Chen., Yinghao, Miao., Qiuhan, Li., Yue, Qin, Hou., Linbing, Wang. (2022). Data Augmentation and Intelligent Recognition in Pavement Texture Using a Deep Learning, doi: 10.1109/TITS.2022.3140586

45. Qian, Liu. (2022). Deep learning based GPR images detection of pavement distress. doi: 10.1109/ICMSP55950.2022.9859162

46. Saarenketo T. and T. Scullion (2000), "Road evaluation with ground penetrating radar", Journal of Applied Geophysics, vol. 43, no. 2-4, pp. 119–138.

47. Saúl, Cano-Ortiz., Pablo, Pascual-Muñoz., Daniel, Castro-Fresno. (2022). Machine learning algorithms for monitoring pavement performance. Automation in Construction, doi: 10.1016/j.autcon.2022.104309

48. Shaw M. R., S. G. Millard, T. C. K. Molyneaux, M. J. Taylor, and J. H. Bungey (2005), "Location of steel reinforcement in concrete using ground penetrating radar and neural networks", NDT & E International, vol. 38, no. 3, pp. 203–212.

49. Sihvola, A., (1999), Electromagnetic Mixing Formulas and Applications. IEEE Publishing, London.

50. Sudyka J., L. Krysiński, A. Zofka, T. Mechowski and P. Harasim (2018), "Identification of deep-rooted transverse cracks using Ground Penetrating Radar", IOP Conf. Ser.: Mater. Sci. Eng., 356 012022.

51. Ting, Deng., Yi, Tan. (2023). Efficient Pavement Distress Detection and Visual Management in Lean Construction Based on BIM and Deep Learnin. doi: 10.24928/2023/0230

52. Tosti, Fabio. (2014). "Experimental and theoretical investigation on road pavements and materials through ground-penetrating radar.", Collana delle tesi di Dottorato di Ricerca In Scienze dell'Ingegneria Civile Università degli Studi Roma Tre.

53. Vilbig, R. A. (2013). Air-coupled and ground-coupled ground penetrating radar techniques (Order No. 1548783). Available from ProQuest Dissertations & Theses A&I; ProQuest Dissertations & Theses Global. (1474901291). https://www.proquest.com/dissertations-theses/air-coupled-ground-penetrating-radar-techniques/docview/1474901291/se-2

54. Wang, C. Y., Yeh, I. H., & Liao, H. Y. M. (2021), "You Only Learn One Representation: Unified Network for Multiple Tasks", arXiv preprint arXiv:2105.04206.

55. Wen, Qiang, Wu., Yihui, Jin. (2023). A Method to Detect Pavement Surface Distress Based on Improved U-Net Semantic Segmentation Network. doi: 10.1109/CVIDL58838.2023.10165980

56. Zhouyan, Qiu., Joaquín, Martínez-Sánchez., Pedro, Arias., Mihai, Datcu. (2023). A novel low-cost multi-sensor solution for pavement distress segmentation and characterization at night. International Journal of Applied Earth Observation and Geoinformation, doi: 10.1016/j.jag.2023.103331